Biomedicine & Pharmacotherapy 171 (2024) 116149

Contents lists available at ScienceDirect

Biomedicine & Pharmacotherapy

journal homepage: www.elsevier.com/locate/biopha

Suppression of metastatic organ colonization and antiangiogenic activity of the orally bioavailable lipid raft-targeted alkylphospholipid edelfosine

Verónica Alonso-Pérez [a], Vanessa Hernández [b], Marco A. Calzado [c,d,e], Alba Vicente-Blázquez [f,g], Consuelo Gajate [a,f], Rafael Soler-Torronteras [c,d,e], Kathleen DeCicco-Skinner [g], Angels Sierra [b,h,i], Faustino Mollinedo [a,f,*]

[a] Instituto de Biología Molecular y Celular del Cáncer (IBMCC), Centro de Investigación del Cáncer (CIC), Consejo Superior de Investigaciones Científicas (CSIC)-Universidad de Salamanca, Campus Miguel de Unamuno, E-37007 Salamanca, Spain
[b] Biological Clues of the Invasive and Metastatic Phenotype Group, Molecular Oncology Department, Bellvitge Biomedical Research Institute (IDIBELL), E-08907 L'Hospitalet de Llobregat, Barcelona, Spain
[c] Instituto Maimónides de Investigación Biomédica de Córdoba (IMIBIC), E-14004 Córdoba, Spain
[d] Departamento de Biología Celular, Fisiología e Inmunología, Universidad de Córdoba, E-14004 Córdoba, Spain
[e] Hospital Universitario Reina Sofía, E-14004 Córdoba, Spain
[f] Laboratory of Cell Death and Cancer Therapy, Department of Molecular Biomedicine, Centro de Investigaciones Biológicas Margarita Salas, CSIC, C/ Ramiro de Maeztu 9, E-28040 Madrid, Spain
[g] Department of Biology, American University, Washington, DC 20016, USA
[h] Laboratory of Experimental Oncological Neurosurgery, Neurosurgery Service, Hospital Clinic de Barcelona-FCRB, E-08036 Barcelona, Spain
[i] Department of Medicine and Life Sciences (MELIS), Faculty of Health and Live Sciences, Universitat Pompeu Fabra, E-08036 Barcelona, Spain

ARTICLE INFO

Keywords:
Metastatic organ colonization
Metastasis
Angiogenesis
Antitumor activity
Edelfosine
Alkylphospholipid analog
Ether lipid
Lipid raft

ABSTRACT

Metastasis is the leading cause of cancer mortality. Metastatic cancer is notoriously difficult to treat, and it accounts for the majority of cancer-related deaths. The ether lipid edelfosine is the prototype of a family of synthetic antitumor compounds collectively known as alkylphospholipid analogs, and its antitumor activity involves lipid raft reorganization. In this study, we examined the effect of edelfosine on metastatic colonization and angiogenesis. Using non-invasive bioluminescence imaging and histological examination, we found that oral administration of edelfosine in nude mice significantly inhibited the lung and brain colonization of luciferase-expressing 435-Lung-eGFP-CMV/Luc metastatic cells, resulting in prolonged survival. In metastatic 435-Lung and MDA-MB-231 breast cancer cells, we found that edelfosine also inhibited cell adhesion to collagen-I and laminin-I substrates, cell migration in chemotaxis and wound-healing assays, as well as cancer cell invasion. In 435-Lung and other MDA-MB-435-derived sublines with different organotropism, edelfosine induced G_2/M cell cycle accumulation and apoptosis in a concentration- and time-dependent manner. Edelfosine also inhibited *in vitro* angiogenesis in human and mouse endothelial cell tube formation assays. The antimetastatic properties were specific to cancer cells, as edelfosine had no effects on viability in non-cancerous cells. Edelfosine accumulated in membrane rafts and endoplasmic reticulum of cancer cells, and membrane raft-located CD44 was downregulated upon drug treatment. Taken together, this study highlights the potential of edelfosine as an attractive drug to prevent metastatic growth and organ colonization in cancer therapy. The raft-targeted drug edelfosine displays a potent activity against metastatic organ colonization and angiogenesis, two major hallmarks of tumor malignancy.

Abbreviations: APL, alkylphospholipid analog; BBB, blood-brain barrier; BLI, bioluminescence imaging; BODIPY, boron-dipyrromethene; ET-18-OCH_3, 1-*O*-octadecyl-2-*O*-methoxy-*rac*-glycero-3-phosphocholine (edelfosine); Et-BDP-ET, 1-*O*-[11''-(6''-ethyl-1'',3'',5'',7''-tetramethyl-4'',4''-difluoro-4''-bora-3a'',4a''-diaza-*s*-indacen-2''-yl)undecyl]−2-*O*-methyl-*rac*-glycero-3-phosphocholine; FBS, fetal bovine serum; H&E, hematoxylin and eosin; HBMECs, human brain microvascular endothelial cells; HUVECs, human umbilical vein endothelial cells; MTT, 3-(4,5-dimethylthiazol-2-yl)− 2,5-diphenyltetrazolium bromide; RFP, red fluorescent protein.

* Corresponding author at: Laboratory of Cell Death and Cancer Therapy, Department of Molecular Biomedicine, Centro de Investigaciones Biológicas Margarita Salas, CSIC, C/ Ramiro de Maeztu 9, E-28040 Madrid, Spain.
E-mail address: fmollin@cib.csic.es (F. Mollinedo).

https://doi.org/10.1016/j.biopha.2024.116149
Received 5 November 2023; Received in revised form 9 January 2024; Accepted 10 January 2024
Available online 24 January 2024

1. Introduction

Metastasis is the leading cause of death among cancer patients, accounting for about 90% of cancer deaths [1,2]. Despite significant progress in detection and treatment of primary tumors, metastatic disease remains a major clinical hurdle in cancer treatment, and the development of novel therapeutics to prevent metastasis is urgently needed to improve patient prognosis and survival [3]. Distant organ infiltration and colonization are the final and most crucial steps of the metastatic cascade [4]. To colonize organs, circulating tumor cells must extravasate from the bloodstream and survive in the new parenchyma, overcoming several obstacles along the way [4]. The mechanism of metastasis is complex and unclear, and most likely involves different cell types [2,5,6]. To metastasize cancer cells must leave their primary site, circulate in the bloodstream, escape cell death, and harness survival signals to proliferate and form secondary tumors [2,4,5]. Invasion of nearby tissue and seeding of tumor cells at distant sites to form metastases, a hallmark of cancer [7], is a central feature of cancer malignancy, and a major target in cancer therapy [8,9]. Cancer cells interact with endothelial and stromal cells, and also with extracellular matrix components in the new microenvironment, attaching and moving along them to seek nutrient supplies and supportive niches to achieve metastatic colonization [10]. In this regard, major signal transduction pathways governing cell adhesion, migration, survival and death have been shown to be dependent on plasma membrane microdomains named lipid rafts [11,12]. In fact, these cholesterol- and sphingolipid-enriched lipid rafts have been involved in cancer metastasis [13–15], and shown to constitute a novel and promising target in cancer therapy [16–21].

The antitumor ether lipid edelfosine (ET-18-OCH_3; 1-*O*-octadecyl-2-*O*-methoxy-*rac*-glycero-3-phosphocholine), which induces apoptosis in a wide variety of cancer cells, while sparing normal cells [22,23], accumulates in lipid rafts in a number of cancer cells, leading to an effective *in vitro* and *in vivo* antitumor activity by the reorganization of raft protein composition [18,24,25]. Edelfosine, the prototype of a family of structurally related antitumor molecules collectively known as alkylphospholipid analogs (APLs), shows the ability to kill a wide array of human cancer cells by affecting the molecular machinery closely involved in cell death [26,27]. *In vivo* approaches show that edelfosine exerts a rather potent antitumor effect without significant side-effects [18,28–30]. Edelfosine accumulates in lipid rafts [18,23,29,31] and the endoplasmic reticulum [30,32–35], putatively through a raft-mediated process [36,37], of cancer cells. Based on our previous studies, and because edelfosine behaved as a potent lipid raft-targeted drug [18,23,38], we reasoned that the ether lipid edelfosine could affect metastatic colonization of cancer cells as well as metastasis-related processes. To test this hypothesis, we examined the effect of edelfosine on an *in vivo* experimental metastasis assay in mice as well as on a series of *in vitro* functional assays of cell adhesion, migration, and angiogenesis. Here, we report that edelfosine displays a potent antimetastatic and antiangiogenic activity, thus expanding and highlighting the metastatic prevention properties of this promising ether-bonded APL.

2. Materials and methods

2.1. Drug

Edelfosine was obtained from R. Berchtold (Biochemisches Labor, Bern, Switzerland). Edelfosine was prepared as 2 or 4 mM stock solutions in cell culture medium or distilled water as previously described [22,39,40]. [^{3}H]Edelfosine (specific activity, 42 Ci/mmol) was synthesized by tritiation of the 9-octadecenyl derivative (Amersham Buchler) [22] and used for lipid raft localization as previously reported [18,31].

2.2. Cell culture

Human MDA-MB-435 cell line was obtained from Dr. A. Sierra (IDIBELL, L'Hospitalet de Llobregat, Barcelona, Spain) [41]. 435-Lung, 435-Brain, 435-Bone and 435-Liver cells, which are metastatic variants of the melanoma cell line MDA-MB-435 cell line to lung, brain, bone, and liver, respectively, were extracted from primary cultures of lung, brain, bone, and liver metastases of the parental highly metastatic MDA-MB-435 cells, originally injected in athymic Balb/c female nude mice, and established after successive *in vivo/in vitro* passages as previously described [41,42] in order to select highly metastatic cells [43–45]. 435-Lung cells, prone to metastasize to lungs, were transduced with retroviral particles that uniformly expressed high levels of enhanced GFP (435-Lung-eGFP-CMV/Luc cells) to be used for non-invasive bioluminescence imaging (BLI) analyses, as previously described [45,46]. Cells were cultured in DMEM F12 medium (Thermo Fisher, Waltham, MA, USA) supplemented with 10% fetal bovine serum (FBS), 5 mM L-glutamine, 100 U/ml penicillin, and 100 μg/ml streptomycin, in a humidified air atmosphere containing 5% CO_2 at 37 °C. The human breast cancer cell line MDA-MB-231 was purchased from the American Type Culture Collection (ATCC) (Manassas, VA, USA) and cultured in DMEM medium (Thermo Fisher), supplemented with 10% FBS, 5 mM L- glutamine, 100 U/ml penicillin, and 100 μg/ml streptomycin, in a humidified air atmosphere containing 5% CO_2 at 37 °C. Human umbilical vein endothelial cells (HUVECs) were maintained in medium 199 supplemented with 20% FBS, 100 U/ml penicillin, 100 μg/ml streptomycin, 2 mM amphotericin B, 2 mM L-glutamine, 10 mM Hepes, 30 mg/ml ECGS, and 100 mg/ml heparin. Human brain microvascular endothelial cells (HBMECs) were maintained in endothelial cell medium (ScienCell, P60104) supplemented with 5% FBS, 1% ECGS and 1% penicillin/streptomycin. 3B-11 mouse endothelial cells were maintained in DMEM medium (Thermo Fisher) supplemented with 10% FBS, 1% penicillin/streptomycin, and 1% GlutaMAX. All cell lines were used before the fourth passage number. All cell lines were tested for mycoplasma contamination using MycoProbe Mycoplasma Detection Kit (R&D Systems, Abingdon, UK).

2.3. Animal model

Athymic nude-BALB/c female mice (24–26 g weight) (Charles-River Laboratories, Wilmington, MA, USA) were housed at the IDIBELL facility in specific-pathogen-free (SPF) conditions, with 20–24 °C cage temperature, 60% relative humidity, and 12–12 h light-dark periods. Animals were allowed free access to UV irradiated water and an adequate sterile diet.

All animal-related procedures were performed in accordance with the National Institute of Health guidelines for the Care and Use of Laboratory Animals, with the approval of the animal care committee (reference 9703). The IDIBELL Animal Care Facility Committee approved all animal studies. No additional ethical approvals or consents were required. Experimental metastasis was generated by tail vein injection of 1×10^6 435-Lung-eGFP-CMV/Luc metastatic cancer cells in 100 μl of HBSS. Mice were randomly assigned to cohorts of 6 mice each after injection. Mice were orally administered with edelfosine (30 mg/kg), or an equal volume of vehicle (water), for 6 consecutive days a week. Treatment was administered by using a flexible and sterile intragastric catheter (Instech Solomon). Animal body weight and any sign of morbidity were monitored. Drug treatment lasted 12 weeks. Animals were euthanized (isoflurane overdose) 24 h after the last drug administration according to institutional guidelines. A necropsy analysis involving distinct organs was carried out.

2.4. Bioluminescence analysis

Inhalatory anesthesia with O_2 and isoflurane mixture was delivered to athymic mice before image acquisition: induction was performed

outside the bioluminescence chamber (4% isoflurane, 2 l/min) and maintenance inside the chamber (2% isofluorane, 2 l/min) during acquisition. Animals were placed in prone position. The photons recorded in the images were quantified and analyzed using Living Image 4.1 image analysis software (Caliper LifeSciences, Hopkinton, MA, USA). The number of photons was expressed as photon counts per second (p/s). The parameter chosen for treatment evaluation was the average radiance (p/s/cm^2/sr). Luciferin solution (D-Luciferin Firefly potassium salt, L-8220–Biosynth AG) was prepared according to the manufacturer's instructions. Intraperitoneal injection of luciferin solution (200 µl/20 g) was applied 10 min before imaging. Background signals were subtracted from all the bioluminescence measurements as part of image analysis. To this end, a healthy mouse (not inoculated with tumor cells) received luciferin solution (200 µl/20 g) intraperitoneally 10 min before imaging.

2.5. Histological analysis

Tissues were fixed in 4% paraformaldehyde in PBS, embedded in paraffin, cut in 2- to 3-µm sections, and stained with hematoxylin and eosin (H&E) (Sigma-Aldrich, St. Louis, MO, USA). All of these procedures were done by independent personnel of the pathology unit of our center. Tumor sections were analyzed by pathologists to look for micrometastasis and metastatic cells. Images were captured using an Olympus BX51 microscope coupled to an Olympus DP70 digital camera.

2.6. Viability and MTT assays

Cell viability was determined by scoring trypan blue (0.04%, Sigma-Aldrich) uptake at the drug concentrations and time indicated in the figures. In the angiogenesis assay, MTT [3-(4,5-dimethylthiazol-2-yl)−2,5-diphenyltetrazolium bromide] metabolization was used to determine cell viability, based on the ability of metabolically active viable cells to transform the water-soluble MTT into an insoluble purple formazan. Briefly, MTT reagent (5 mg/ml, Sigma-Aldrich) was added and incubated for 3 h at 37 °C. The formazan crystals were solubilized by the addition of 100 µl DMSO and the absorbance at 550 nm was measured using a Multifunction Microplate Reader (TECAN GENios Pro). All determinations were carried out in triplicate.

2.7. Adhesion assay

24-well plates (Falcon; Corning Inc., Tewksbury, MA, USA) coated with 1 µg/ml laminin-I (Sigma-Aldrich) and 10 µg/ml collagen-I (Sigma-Aldrich) were washed with PBS and blocked with DMEM/F12 medium containing 2% BSA. Where indicated, cells were pretreated with edelfosine for 6 h. 2×10^5 cells/well in DMEM/F12 were plated in triplicate and incubated for 40 min at 37 °C. Cells were washed with PBS, fixed, and stained with 0.01% crystal violet in PBS. Cells were washed with PBS, solubilized with 1% SDS, and absorbance read at 630 nm.

2.8. Cell migration and invasion assays

Cell migration was assayed using a transwell chamber assay, using Falcon 24-well flat bottom plates and Falcon permeable supports for 24-well plate with 8.0 µm transparent PET membrane (Corning). Cells were seeded in chambers at the density of 2×10^5 cells per well and cultured in 400 µl of DMEM/F12 medium with 10% FBS, while 600 µl of DMEM/F12 medium with 30% FBS and 8 µg/ml insulin (Thermo Fisher) were added to the lower chamber. Cells were allowed to migrate for 36 h (435-Lung) or 16 h (MDA-MB-231), and then migrated cells were fixed with 100% methanol for 30 min. Non-migrated cells were removed by cotton swabs. Then cells on the bottom surface of the membrane were stained with crystal violet for 20 min. To perform cell invasion assay, transwells were coated with Matrigel (Thermo Fisher) and MDA-MB-231 cells were allowed to invade for 16 h. Cell images were obtained under a phase-contrast microscope (Olympus) and ImageJ software (NIH, Bethesda, MD, USA) was used to quantify migrated and invading cells.

2.9. Wound-healing assay

Cells were cultured in 12-well plates until they reached 100% confluence. A scratch was made in the monolayer with a pipette tip to create a "wound", and cells were treated with 10 µg/ml mitomycin for 30 min to stop cell proliferation. Three wounds were made for each sample, and micrographs of the wound areas to determine wound closure were taken at zero time and at 16 h (MDA-MB-231) and 36 h (435-Lung) after scratching using a phase-contrast microscope (Olympus). The percentage of wound closure was quantified and analyzed using ImageJ software.

2.10. Cell cycle analysis

For cell cycle analyses, untreated and drug-treated cells (2–4 $\times 10^5$) were centrifuged and fixed overnight in 70% ethanol at 4 °C. Samples were washed twice with PBS, incubated with 0.2 mg/ml RNase A, 10 µg/ml propidium iodide, and 0.5% NP-40 in 350 µl PBS for 30–60 min at room temperature, and analyzed with a CytomicsTM FC500 flow cytometer (Beckman Coulter, Brea, CA, USA) as previously described [47]. Cell cycle analysis was performed using Cyflogic software (Perttu Terho, Mika Korkeamaki, CyFlo Ltd., Turku, Finland), and quantification of apoptotic cells was calculated as the percentage of cells in the sub-G_0/G_1 region (hypodiploidy) in cell cycle analysis [47].

2.11. Edelfosine subcellular localization by confocal microscopy

The subcellular localization of edelfosine was examined with the edelfosine fluorescent analog 1-*O*-[11'-(6''-ethyl-1'',3'',5'',7''-tetramethyl-4'',4''-difluoro-4''-bora-3a'',4a''-diaza-*s*-indacen-2''-yl) undecyl]− 2-*O*-methyl-*rac*-glycero-3-phosphocholine (Et-BDP-ET) [48], which contains a boron-dipyrromethene (BODIPY) molecule, a kind gift from F. Amat-Guerri and A.U. Acuña (Consejo Superior de Investigaciones Científicas, Madrid, Spain). The endoplasmic reticulum was visualized using the CellLight™ ER-red fluorescent protein (RFP), BacMam 2.0 reagent, following the manufacturer's specifications. This CellLight™ ER-RFP, BacMam 2.0 reagent includes a fusion construct of endoplasmic reticulum signal sequence of calreticulin and KDEL (endoplasmic reticulum retention signal) and TagRFP, providing accurate and specific targeting to cellular ER-RFP, with minimal cellular disruption. Colocalization of both signals (RFP; Excitation: 555 nm, Emission: 574–627 nm; BODIPY: Excitation: 498 nm, Emission: 510–549 nm) was analyzed by excitation of both fluorochromes in the same section. Fluorescence was visualized with a confocal laser scanning microscope Leica TCS SP8 STED 3X, fitted with UV laser 405 nm and white light laser freely tunable excitation from 470–670 nm (Wetzlar, Germany).

2.12. Lipid raft isolation

Lipid rafts were isolated from 6–8 $\times$ 10^7 cells by using nonionic detergent lysis conditions and centrifugation on discontinuous sucrose gradients as previously reported [49]. Eleven fractions (1-ml) were collected from the top of the gradient and 20 µl of each fraction were subjected to SDS-PAGE, immunoblotting and enhanced chemiluminescence, as previously described [49,50]. The lipid raft-enriched fractions were confirmed by Western blot analysis based on the presence and distribution of the lipid raft marker flotillin [51]. Proteins were identified using specific antibodies: anti-flotillin-1 (BD Transduction; catalog number: 610821), HP2/9 anti-CD44 (provided by F. Sánchez-Madrid, Hospital de La Princesa, Madrid, Spain).

2.13. Angiogenesis assay

HUVECs and HBMECs (2×10^4) were seeded over a uniform layer of Matrigel (BD Biosciences, Franklin Lakes, NJ, USA) in a 96-well plate. After 12 h cells were washed with PBS and stained with 5 μg/ml calcein-AM (Thermo Fisher). Tube formation was analyzed using a 4 × objective and a BD Pathway 855 Bioimager. Attovision v 1.7 BD software was used to quantify the total length and branch points of tubes. Tube total length is the total number of pixels comprising the network in the image field.

3B-11 cells (18×10^4) were seeded in conditioned media over a uniform layer of growth factor reduced BME (Corning) in a 24-well plate. Before conducting the assay, 3B-11 cells were starved overnight in DMEM supplemented with 0.2% FBS, 1% penicillin/streptomycin, and 1% GlutaMAX, and stained with 2 μg/ml calcein-AM for 30 min. Tube formation was analyzed after 6 h under an Olympus SZX16 dissection scope. ImageJ software (Angiogenesis Analyzer Plugin, HUVEC Fluo Analysis) was used to quantify the number of nodes, meshes, and segments as previously described [52].

2.14. Statistical analysis

The *in vitro* results are shown as the mean ± SD of 5–10 independent experiments. Statistical evaluation was performed by non-parametric mixed-effects analysis model with Dunnett's multiple comparisons test, or by Student's t-test. A p-value lower than 0.05 was considered statistically significant. *In vivo* data were expressed as mean ± SD. Survival curves were estimated *via* the Kaplan-Meier method, and the Log-Rank test was used to assess if they were significantly different. Tumor burden and brain and lung metastasis curves were estimated by non-parametric Multiple Mann-Whitney tests followed by Holm-Sidak's adjustment. *P*-values lower than 0.05 were considered significant.

3. Results

3.1. Edelfosine inhibits metastatic organ colonization of cancer cells

To investigate the effect of edelfosine on metastatic organs, we first performed an *in vivo* experimental metastasis assay, using the luciferase-expressing 435-Lung-eGFP-CMV/Luc lung metastatic cells [45]. This metastatic variant 435-Lung cell line was established from cultures of lung metastases generated in athymic Balb/c female nude mice, originally injected with MDA-MB-435 melanoma cells, and following successive *in vivo/in vitro* passes as previously described [41,42] in order to select highly metastatic cells [43,45]. Athymic nude mice were tail vein-injected with these 435-Lung-eGFP-CMV/Luc cells and treated with orally administered edelfosine for 12 weeks (starting treatment 5 days after injection of cancer cells) (Fig. 1a). We monitored 435-Lung-eGFP-CMV/Luc cells by non-invasive BLI, determining a cranial region as brain metastasis, thoracic region as lung metastasis and entire body as total tumor burden (Fig. 1b). In untreated control mice, high loads of 435-Lung cancer cells were found close to the site of injection as well as in lung and brain after 33 (mouse 5), 46 (mouse 1), 53 (mouse 2), 75 (mice 4 and 6), and 89 (mouse 3) days (Fig. 1c). Thus, 435-Lung cells metastasized efficiently to the brain in addition to lung (Fig. 1c). In sharp contrast, proliferation of metastatic 435-Lung cells injected into the circulation of mice, as well as brain and lung metastasis, were dramatically inhibited in edelfosine-treated mice compared with control counterparts (Fig. 1, c and d). Edelfosine oral treatment led to a dramatic decrease in the total tumor burden (Fig. 1e). Further, there was 100% survival of tumor-bearing mice (Fig. 1f), as compared to non-treated mice. Brain metastases were completely suppressed in all mice of the drug-treated group, and lung metastases were inhibited in five out of the six mice used in these experiments (Fig. 1, c and d). These results were validated by histological staining, with no brain metastases in edelfosine-treated mice after processing multiple consecutive brain sections (Fig. 2a). Similar histological results were obtained with lung metastases (Fig. 2b), and only lung micrometastasis could be detected in one of the six edelfosine-treated mice (Fig. 2b). Edelfosine treatment did not induce any adverse effects on mice, as assessed by no weight loss (Supplementary Fig. S1), as well as by normal histological features of the brain, lung and liver tissue sections (Fig. 2, and Supplementary Fig. S1). Taken together, our BLI and histological data indicate that oral administration of edelfosine dramatically inhibits the growth of 435-Lung-eGFP-CMV/Luc metastatic cells in the lungs and brain, the most frequent organs of melanoma distant metastases [53].

3.2. Concentration-response and time-course effects of edelfosine on cell cycle and apoptosis in 435 metastatic cancer cells

Previous data have shown that edelfosine is able to induce apoptosis in the range of 10–20 μM in many different human tumor cells, including distinct hematological cancer cells [16,23,25,54], various solid-derived tumor cells [30,55], as well as pancreatic cancer stem cells [34]. Here, using flow cytometry assays, we found that metastatic 435-Lung melanoma cells were rather resistant to edelfosine, as they do not undergo significant apoptosis with 20 μM edelfosine after even protracted incubation times (Fig. 3a), and only a cell cycle accumulation at G_2/M was detected after 24 h incubation at 20 μM (Fig. 3a). Time-course and concentration-response analyses showed that 50 μM edelfosine induced a significant G_2/M cell cycle accumulation after 24 h incubation, followed by the subsequent onset of apoptosis after 48–72 h incubation in 435-Lung cells (Fig. 3b). These changes were more evident at 75 μM edelfosine (Fig. 3b). These results showed that the G_2/M cell cycle accumulation and subsequent apoptosis response were highly dependent on drug concentration and incubation time, and drug concentrations over 20 μM and protracted times were required to highlight the above changes.

Similarly to 435-Lung cells, different 435 sublines were selected for their tropism to bone (435-Bone), brain (435-Brain), and liver (435-Liver) [41,43,45,56]. These latter cell lines underwent a cell cycle accumulation at G_2/M and subsequent apoptosis at concentrations $\geq$ 20 μM and after protracted incubations (Fig. 3c). These metastatic cells were found to be more sensitive than the 435-Lung cells to edelfosine. The sensitivity of the above different metastatic cells to undergo G_2/M cell cycle accumulation and apoptosis ranked 435-Brain > 435-Liver > 435-Lung > 435-Bone cells (Fig. 3c).

It might be questioned that the rather high concentration of edelfosine required to elicit apoptosis in these 435 metastatic cancer cells (Fig. 3) could lead to a nonspecific or detergent effect on membranes. However, we found that the inactive edelfosine analogs 1-*O*-octadecyl-*rac*-glycero-3-phosphocholine (ET-18-OH) or 1-*O*-octadecyl-propanediol-3-phosphocholine (ET-18-H) [22,54,57], which were closely structurally related analogs by replacing the methoxy group in the *sn*-2 position by an OH (ET-18-OH) or H (ET-18-H), had no effect on either cell cycle or cell death, even at 75 μM in the different 435 cell sublines (< 4% apoptosis). This indicates that the apoptotic response induced by edelfosine, even at the above high concentrations, was specific of its molecular structure and was not due to a non-specific drug effect. On the other hand, we have previously found that edelfosine shows a weak detergent activity, which could be related to its low critical micellar concentration [58].

We also found that the parental MDA-MB-435 cell line underwent G_2/M accumulation and apoptosis upon edelfosine treatment, similarly to the distinct 435 metastatic sublines, but it showed a slightly higher sensitivity to the ether lipid (18.7 ± 1.8% apoptosis and 58.3 ± 4.7% cells accumulated at G_2/M after 24 h incubation with 20 μM edelfosine). This is in agreement with previous studies carried out with the cell line MDA-MB-435s, showing a reduction in cancer cell proliferation and the accumulation of cells in the G_2/M phase of the cell cycle following edelfosine treatment at even low micromolar concentrations of edelfosine [59]. This apparently higher resistance of the metastatic sublines is in consonance with the notion that dormant disseminated cancer cells

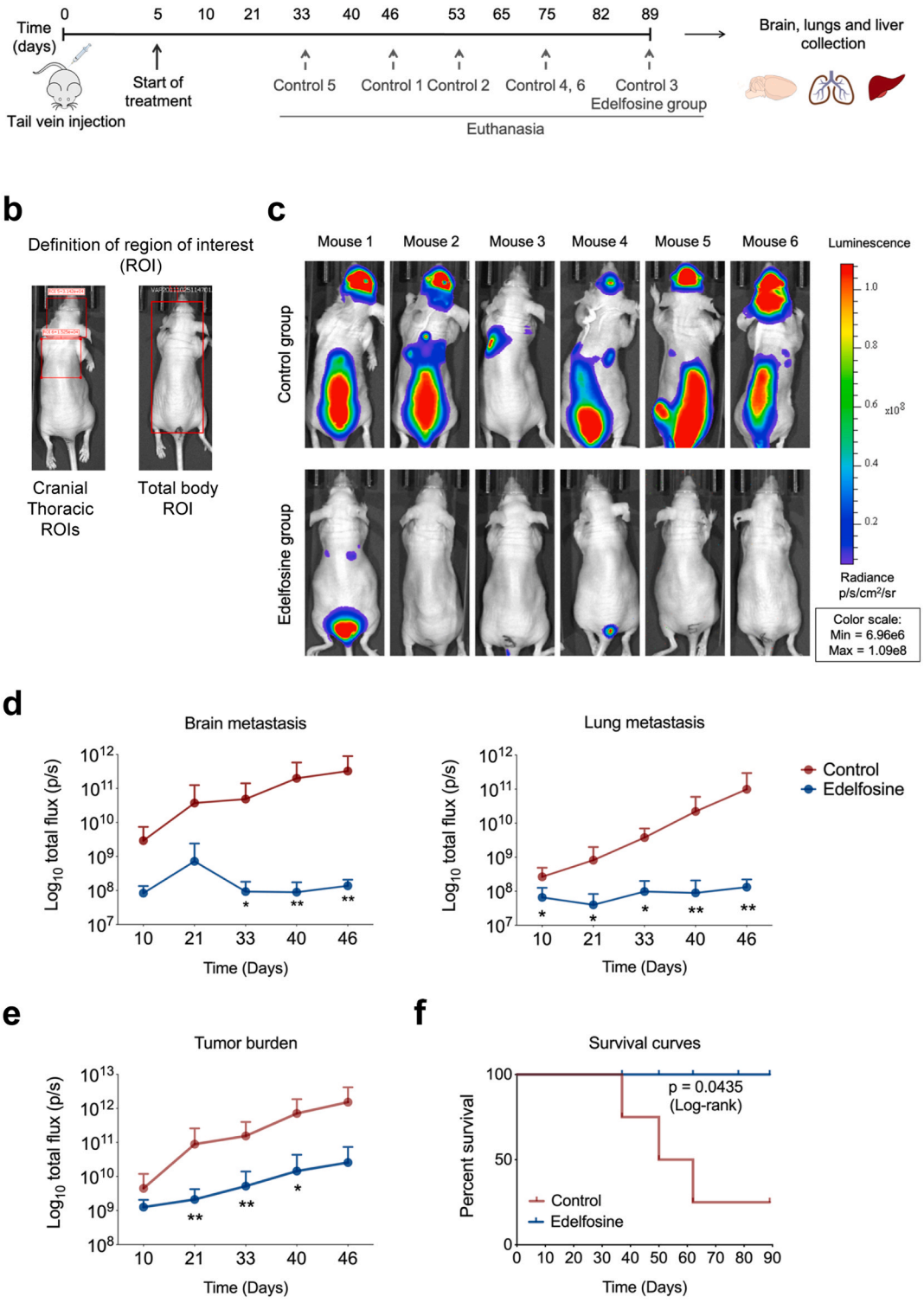

Fig. 1. Edelfosine inhibits metastatic organ colonization. (**a**) Experimental design. Luciferase-expressing 435-Lung-eGFP-CMV/Luc cancer cells were injected into the tail vein of immunodeficient female mice on day 0. Mice were randomized into 2 cohorts ($n = 6$), untreated control and edelfosine-treated group. Edelfosine treatment started on day 5 and was orally administered for 6 consecutive days per week during 12 weeks. Control group was treated with the same volume of vehicle (water). Treatment finished on day 89. Mice were weighed and monitored weekly using bioluminescent imaging (BLI) and gross observation for clinical signs of metastatic disease. BLI images were taken at the times indicated at the top of the scheme, and mice with signs of illness were euthanized on the days indicated at the bottom of the scheme. All mice from the edelfosine-treated group and mouse 3 from the untreated control group were euthanized on day 89. (**b**) Different regions of interest (ROIs) were defined in the IVIS Imaging software to measure total bioluminescent signal or flux in the cranial, thoracic and total body areas. (**c**) BLI images corresponding to the endpoint for each mouse in the untreated control group (top) and edelfosine-treated group (bottom). (**d**) Quantification (total flux, photons per second, p/s) of the bioluminescent signal from brain (left) and lung (right) metastasis as measured by BLI in the untreated control group (red) and edelfosine-treated group (blue). (**e**) Time-course of tumor burden as measured by BLI in the untreated control group (red) and edelfosine-treated group (blue). (**f**) Kaplan-Meier curves of survival for untreated control group (red) and edelfosine-treated group (blue), $p = 0.0435$ (log-rank test). Graphs in **d** and **e** include values until day 46 of the experiment (untreated control group, $n = 5$; edelfosine-treated treated group, $n = 6$). Data are presented as mean (SD), *$p < 0.05$, **$p < 0.01$.

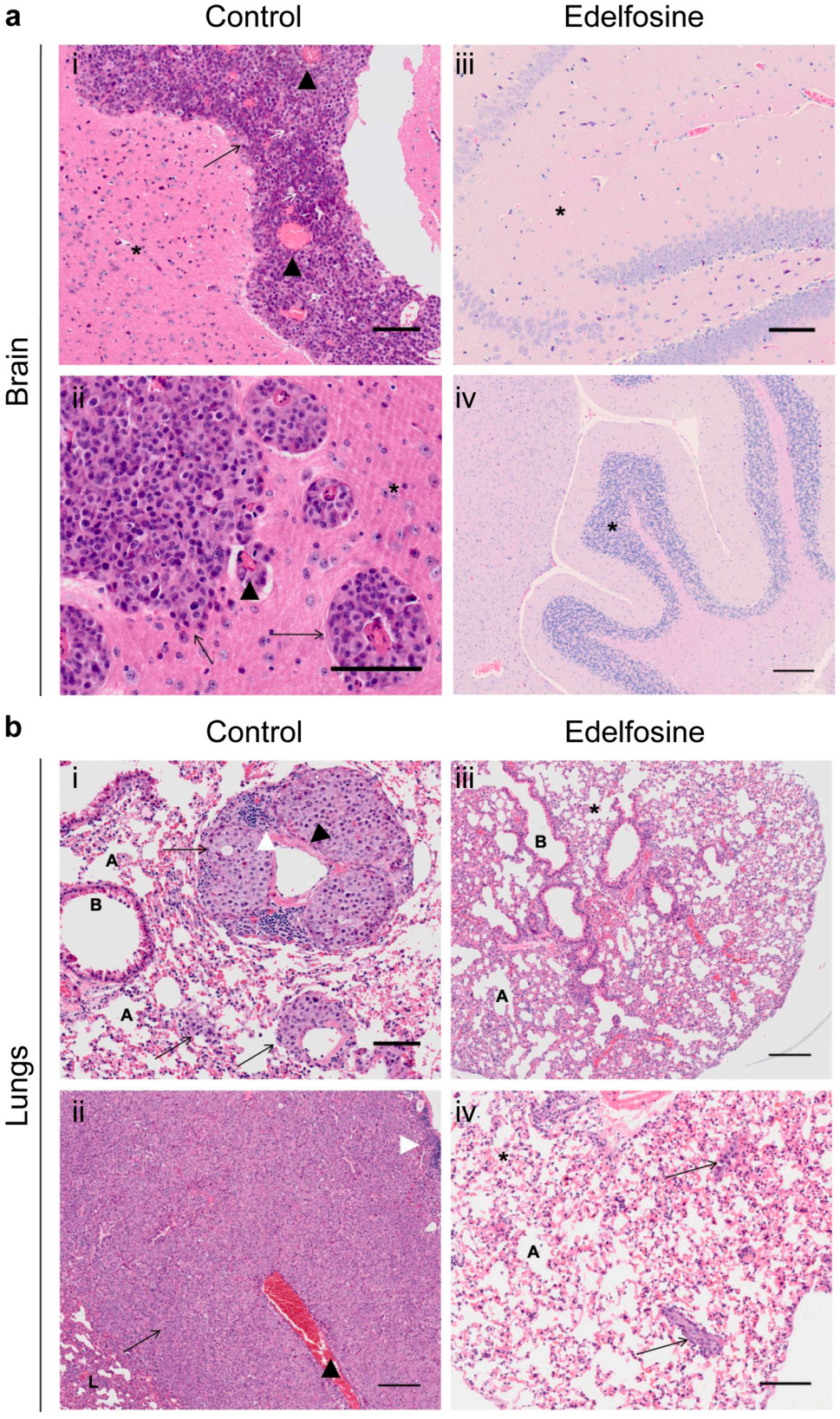

(caption on next page)

Fig. 2. Histological analysis validates BLI results. Representative HE (hematoxylin and eosin) images of brain (**a**) and lungs (**b**) in untreated control group (**i**, **ii**) and edelfosine-treated group (iii, iv). (**a-i**) Brain of control mouse. Brain parenchyma (asterisk) replaced by a mass of atypical tumor cells (arrows) with presence of mitotic figures (white arrows) and vessels (arrow head). HE, 10x. Scale bar, 100 μm. (**a-ii**) (Detail) Brain of control mouse. Tumor cells (arrows) with atypical signs, nuclei with different sizes, evident nucleoli and scarce eosinophilic cytoplasms, surrounded by neuronal cells (asterisk). Vessel (arrow head). HE, 20x. Scale bar, 150 μm. (**a-iii**) Brain of edelfosine-treated mouse. Hippocampus of an edelfosine-treated mouse. Histological structure is preserved (asterisk) with no infiltration of tumor cells. HE, 10x. Scale bar, 100 μm. (**a-iv**) Brain of edelfosine-treated mouse. Cerebellum of an edelfosine-treated mouse. Histological structure is preserved (asterisk) with no infiltration of tumor cells. HE, 10x. Scale bar, 100 μm. (**b-i**) Lungs of a control mouse. Tumor perivascular nodules (arrows) with chronic lymphocitic inflammation (white arrow head) and isolated tumor cells (arrows). Preserved lung tissue with terminal bronchiole (B) and air sacs (A). HE, 10x. Scale bar, 100 μm. (**b-ii**) Lungs of a control mouse. Tumor mass (arrow) with a central blood vessel (arrow head) surrounded by chronic lymphocitic inflammatory reaction (white arrow head) and lung tissue (L). HE 2x. Scale bar, 500 μm. (**b-iii**) Lungs of edelfosine-treated mouse. Preserved lung tissue (asterisk) with no infiltration of tumor cells. Terminal bronchiole (B). Air sacs (A). HE, 2x. Scale bar, 100 μm. (**b-iv**) Lungs of the only edelfosine-treated mouse (one out of six) showing micrometastasis. Preserved lung tissue (asterisk) with infiltration of tumor cells (arrows) confirming micrometastases. Air sacs (A). HE, 4x. Scale bar, 150 μm.

and micrometastases show a generalized resistance to chemotherapy and immunotherapy, which underpins the current difficulties in eradicating cancer and remains a challenge in oncology [60,61].

3.3. Edelfosine inhibits cancer cell adhesion and migration properties

Metastasis and invasive tumor growth involve a series of critical steps, including cell adhesion and migration along the substrate, which constitute important points in the control of cancer progression [2]. Thus, we next analyzed the action of edelfosine on these functions in order to elucidate the underlying basis of the potent *in vivo* antimetastatic effect of edelfosine shown above.

First, we analyzed cell adhesion to two pivotal substrates in the tumor microenvironment required for the generation of secondary tumors, namely collagen-I and laminin-I, which are the main components of the extracellular matrix and basement membrane in tissues and blood vessels, respectively [62]. We found that edelfosine induced a potent concentration-dependent inhibition of cell adhesion in 435-Lung cells (Fig. 4), without impairing cell viability, as assessed by the MTT cell proliferation assay (Supplementary Fig. S2). Edelfosine significantly inhibited cell adhesion, starting at low drug concentrations, such as 5 and 10 μM, which had no effect on cell cycle or apoptosis induction (Fig. 3). Next, we evaluated the effect of edelfosine on cell migration. As shown in Fig. 5, edelfosine effectively inhibited cell migration of 435-Lung cancer cells, as assessed by wound-healing assays (Fig. 5, a and b), and chemotaxis using a Boyden chamber migration assay with a chemoattractant (insulin + FBS) gradient (Fig. 5, c and d). While 435-Lung cells closed the wound in 36 h, edelfosine treatment impaired wound closure in a concentration-dependent manner (Fig. 5, a and b) without affecting cell viability (Supplementary Fig. S3).

In order to generalize the above results to additional cancer cells, we also used MDA-MB-231 cell line, which is a highly aggressive, invasive, and poorly differentiated triple-negative breast cancer cell line [63]. This cell line was derived from the pleural effusion of a breast cancer patient suffering from widespread metastasis years after removal of her primary tumor [64]. Similarly to what happened with 435-Lung cells, we found that edelfosine induced a potent concentration-dependent inhibition of cell adhesion in MDA-MB-231 cells (Fig. 4, a and b), without impairing cell viability (Supplementary Fig. S2). Furthermore, we also found that edelfosine effectively inhibited migration of MDA-MB-231 cells, as determined by wound-healing assays (Fig. 5, a and b), and a Boyden chamber assay using a chemoattractant (insulin + FBS) gradient (Fig. 5, c and d). MDA-MB-231 cells closed the wound in 16 h, and edelfosine treatment impaired wound closure in a concentration-dependent manner (Fig. 5, a and b). In the wound-healing assays with both cell types, cell proliferation was inhibited by mitomycin before edelfosine treatment, so the drug affected cell migration without affecting viability (Supplementary Fig. S3). In addition, edelfosine also inhibited MDA-MB-231 cell invasion (Fig. 5e), under experimental conditions that did not induce apoptosis (less than 3% apoptosis in the same experimental conditions). Thus, these results parallel the 435-Lung and MDA-MB-231 cancer cell migration data.

Taken together, these results indicate that edelfosine suppresses cancer cell adhesion and migration, thus impairing two major metastatic properties of cancer cells.

3.4. Edelfosine accumulates in lipid rafts and endoplasmic reticulum in metastatic cancer cells

Because edelfosine has been shown to accumulate in lipid rafts and endoplasmic reticulum in distinct human tumor cells [18,23,30,31,34], we examined the subcellular localization of edelfosine in 435-Lung cells following a 3 h incubation period. The fluorescent edelfosine analog 1-*O*-[11′-(6′′-ethyl-1′′,3′′,5′′,7′′-tetramethyl-4′′,4′′-difluoro-4′′-bora-3a′′,4a′′-diaza-*s*-indacen-2′′-yl)undecyl]− 2-*O*-methyl--*rac*-glycero-3-phosphocholine (Et-BDP-ET), previously used to identify the subcellular location of edelfosine [34,36,48], accumulated in the endoplasmic reticulum of the 435-Lung cells (Fig. 6a). Furthermore, [^{3}H]edelfosine accumulated in lipid raft fractions from 435-Lung cells (fractions 3–5 in Fig. 6b), defined by their enrichment in flotillin, which is used as a lipid raft marker [51]. Interestingly, CD44, which is suggested to play a major role in cell migration and metastasis [12,65], was mainly found in the lipid raft fractions (Fig. 6c), and its cell surface expression was downregulated upon edelfosine treatment (Fig. 6d). Altogether, these results suggest that edelfosine may target membrane lipid rafts, resulting in CD44 downregulation and impairment of metastasis-related processes.

3.5. Edelfosine inhibits angiogenesis in human and mouse models

Because angiogenesis is crucial for metastatic progression from micrometastases to macroscopic metastases [66], we next examined the anti-angiogenic effect of edelfosine using tube formation assays with human brain microvascular endothelial cells (HBMECs) and human umbilical vein endothelial cells (HUVECs). We found that edelfosine diminished the mesh number and the total tube length in both cell types (Fig. 7, a and b). Furthermore, edelfosine did not affect cell viability under the experimental conditions (12-h incubation) used for the tube formation assay, as assessed by the MTT cell proliferation assay (Fig. 7c).

In addition, edelfosine also inhibited tube formation of 3B-11 mouse endothelial cells after 6-h incubation (Fig. 7, d and e), although at higher drug concentrations than in human endothelial cells (Fig. 7, a and d), preventing the tube formation at 50 μM drug concentration, as assessed by measuring the number of nodes, meshes and segments. No detrimental effect on cell viability was observed under the above experimental conditions, as assessed by the MTT cell proliferation assay (>95% cell viability after incubation with 10, 20 or 50 μM edelfosine for the incubation time of the angiogenesis experiment, *i.e.*, 6 h).

These results suggest that edelfosine does not induce cell death in normal endothelial cells, further supporting previous studies reporting that this ether lipid promotes apoptosis in cancer cells while sparing normal cells [22,23,25].

4. Discussion

The results reported here suggest a potent antimetastatic action of

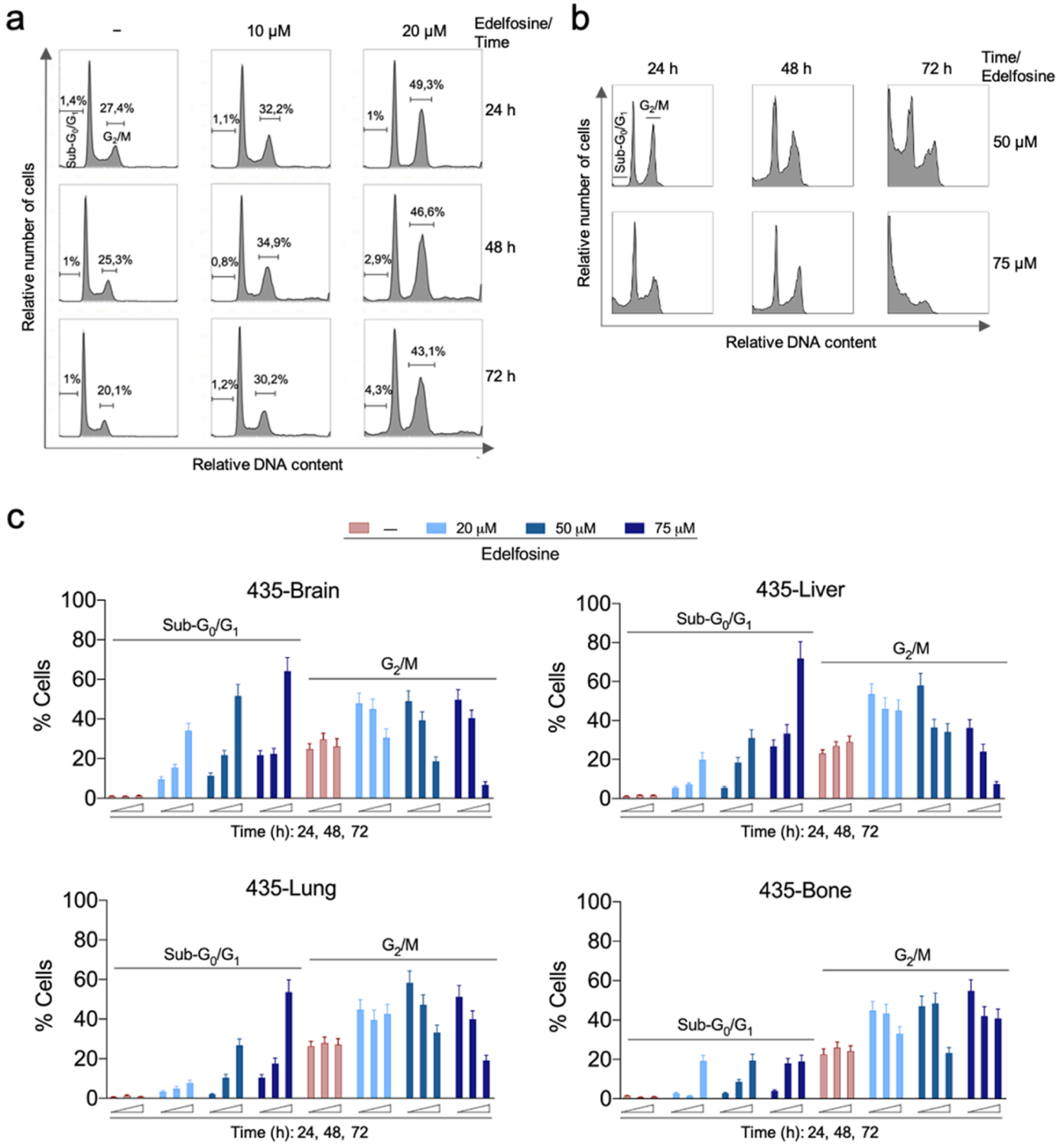

Fig. 3. Time-course and concentration-dependent effects of edelfosine on cell cycle and apoptosis in 435-Lung cancer cells and different organotropic MDA-MB-435 cancer cell variants. (**a**) 435-Lung cancer cells were untreated or treated with 10 or 20 μM edelfosine for the indicated times, and then DNA content was analyzed by cell cycle analysis. The percentage of cells at the hypodiploid region (Sub-G_0/G_1), corresponding to apoptotic cells, and at G_2/M phase (right) are indicated in each histogram. Data shown are representative of at least three independent experiments. **(b)** Metastatic 435-Lung cells were incubated for different incubation times in the absence (*Control*) or presence of different concentrations of edelfosine (*Edelfosine*) as indicated, and then cell cycle in propidium iodide-stained cells was analyzed by flow cytometry. The percentages of cells at sub-G_0/G_1 and at the G_2/M regions are indicated in each histogram. Cell cycle profiles shown are representative of five experiments performed. **(c)** 435-Brain, 435-Lung, 435-Liver, and 435-Bone cells were incubated in the absence *(Control)* or presence of different concentrations of edelfosine (*Edelfosine*) for the indicated times, and the percentage of cells accumulated at G_2/M and undergoing apoptosis (sub-G_0/G_1, hypodiploidy) were determined by flow cytometry. Data shown are means (SD) of five independent experiments.

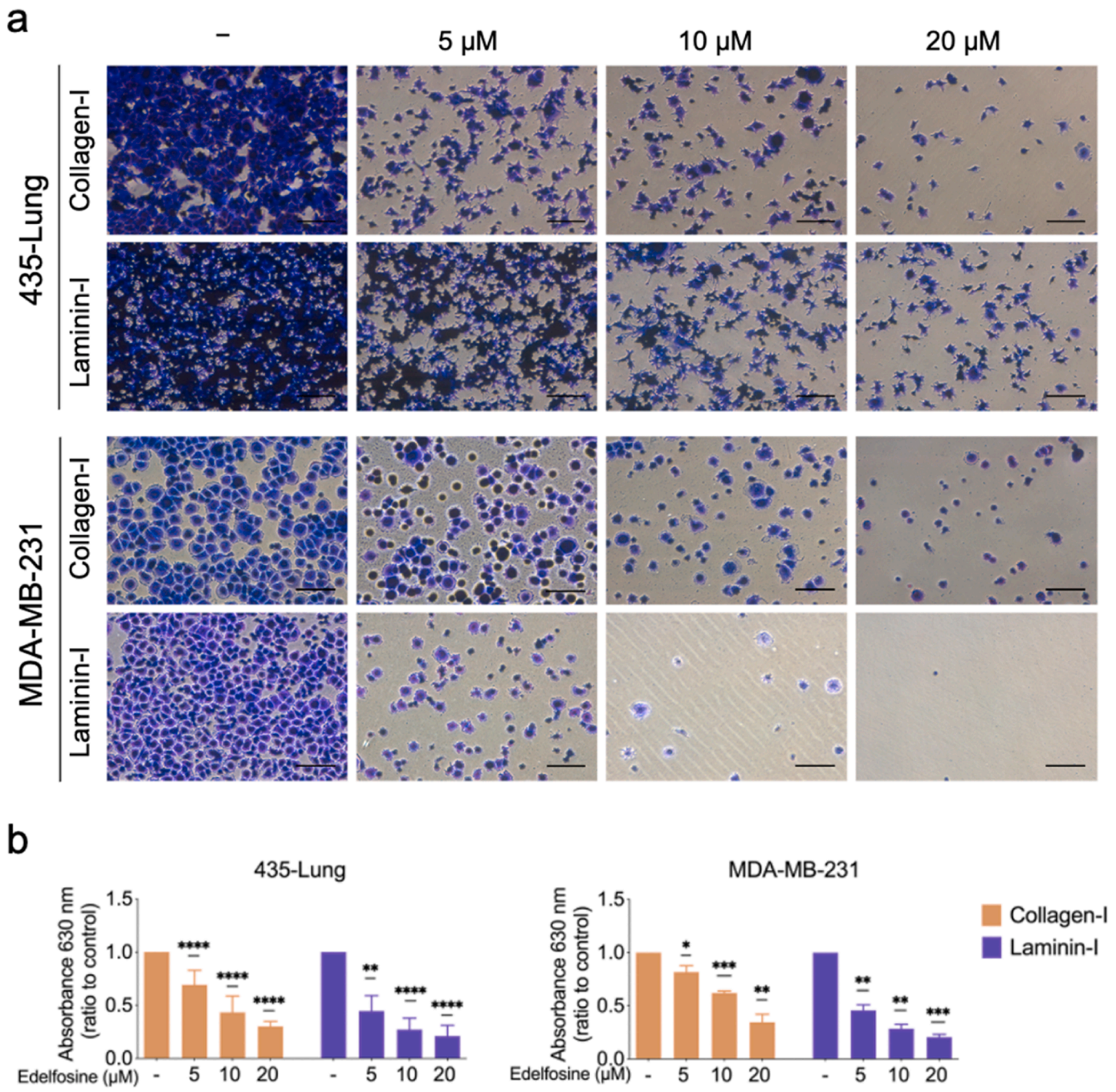

Fig. 4. Edelfosine inhibits cell adhesion of 435-Lung and MDA-MB-231 cancer cells. (**a**) Representative images of cell adhesion assays with 435-Lung (*Upper panels*) and MDA-MB-231 (*Lower panels*) cancer cells, following treatment with increasing concentrations of edelfosine for 6 h and then allowed to attach to collagen-I and laminin-I coated plates. After 40 min of incubation at 37 °C, cells were stained with violet crystal, and (**b**) Quantitative results of cell adhesion assays for 435-Lung (*Left panel*) and MDA-MB-231 (*Right panel*) cells were determined by absorbance at 630 nm after solubilization with SDS. Cell images were obtained under phase-contrast microscopy, and cells were counted with ImageJ software. Images in **a** panels were taken at 20x magnification; scale bar: 100 μm. At least three independent experiments were performed in each group. Data are shown as mean ± SD. *p < 0.05, **p < 0.01, ***p < 0.001, ****p < 0.0001.

edelfosine in cancer cells, which includes its inhibitory effect on cancer cell adhesion and migration, as well as on angiogenesis, and the accumulation of metastatic cancer cells in G_2/M cell cycle followed by apoptosis after prolonged drug incubation. Using an established *in vivo* tail vein injection model in athymic nude mice [67,68], together with a non-invasive BLI method to quantify tumor and metastasis burden, we assessed the metastatic capacity of luciferase-expressing 435-Lung cancer cells. Here we found that edelfosine oral treatment, used at pharmacologically active doses [18,69], was highly effective in preventing metastatic spread, as no edelfosine-treated mice developed brain metastases and only one animal developed a lung micrometastasis. Furthermore, while 83% of control mice died within 90 days, 100% of edelfosine-treated mice survived for the duration of the study. Histological staining of paraffin-embedded tissue sections further demonstrated the absence of brain and lung metastasis in drug-treated mice.

According to our experimental design (Fig. 1a), we initiated edelfosine oral treatment (6 days/week, Monday to Saturday, once daily) 5 days after injection of 435-Lung-eGFP-CMV/Luc cancer cells into the vein of immunodeficient mice, and then BLI measurements started 5 days after drug treatment (Fig. 1a). It has been previously determined

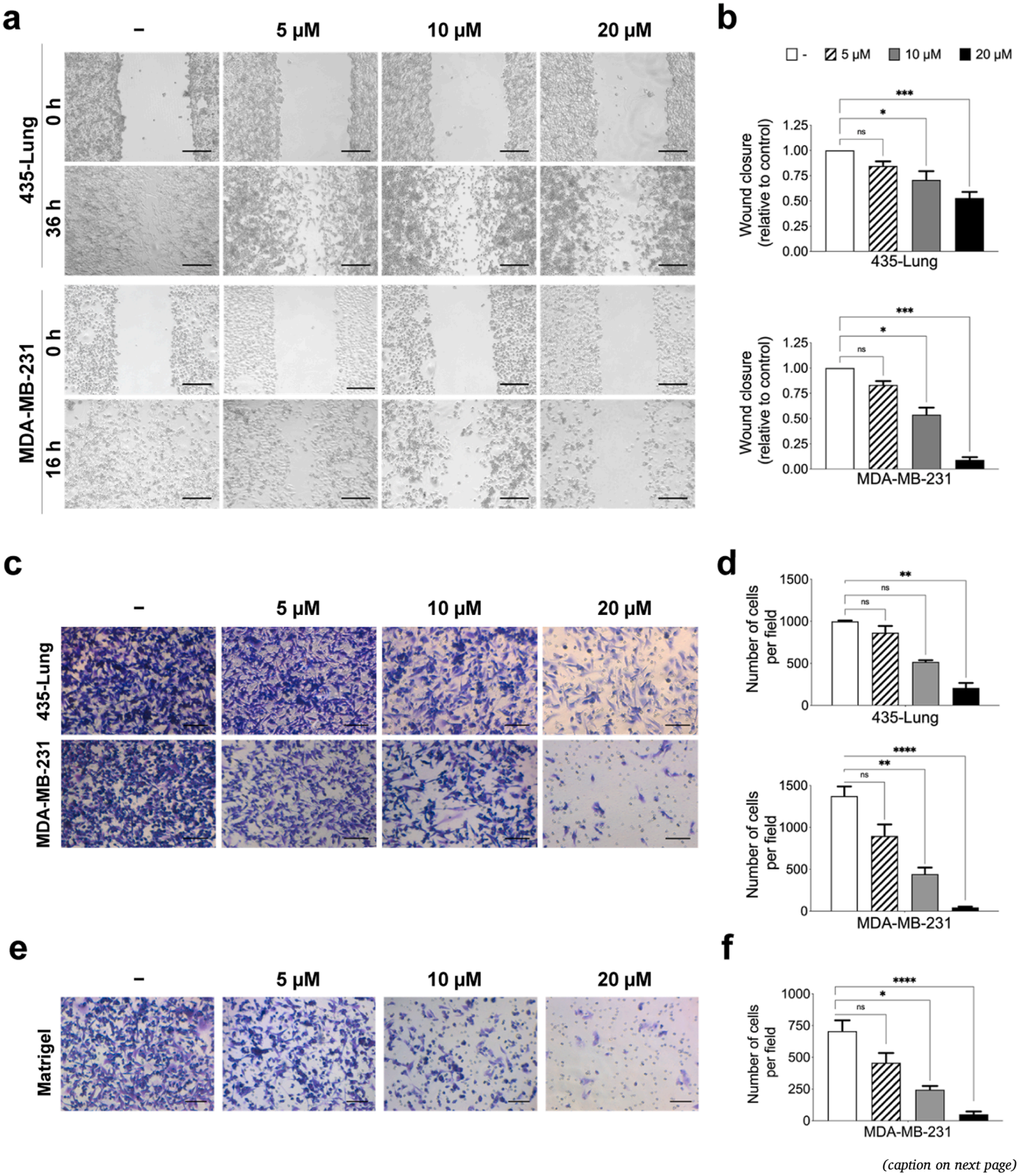

(caption on next page)

Fig. 5. Edelfosine inhibits cell migration in 435-Lung melanoma cells and triple-negative MDA-MB-321 breast cancer cells. (**a**) Representative images of a wound-healing assays. 435-Lung (*Upper panels*) and MDA-MB-231 (*Lower panels*) cells were grown to confluence and proliferation was inhibited by treatment with 10 μg/ml mitomycin before edelfosine treatments. Monolayers were scrapped with a 10 μl pipette tip and washed with culture medium to remove non-adherent cells. Then culture medium was added with increasing concentrations of edelfosine as indicated for 36 h (435-Lung) and 16 h (MDA-MB-231). Images were obtained under a phase-contrast microscopy at 0 (*upper*) and 36 h (*lower*) for 435-Lung cells and at 0 (*upper*) and 16 h (*lower*) for MDA-MB-231 cells. (**b**) Wound closure areas were measured by ImageJ software and normalized to untreated controls. (**c**) Representative images of Boyden chamber migration assays. 435-Lung (*Upper panel*) and MDA-MB-231 (*Lower panel*) cells, untreated and treated with the indicated concentrations of edelfosine, were seeded on culture inserts and allowed to migrate in a gradient of FBS plus insulin for 36 h (435-Lung) or 16 h (MDA-MB-231). Migrated cells were fixed with 100% methanol for 30 min. Non-migrated cells were removed by cotton swabs. Then, cells on the bottom surface of the membrane were stained with crystal violet for 20 min (**d**) Quantitative results of cell migration assays for 435-Lung and MDA-MB-231 cells were obtained by cell counting. (**e**) Representative images of a Matrigel-invasion assay. MDA-MB-231 cells, untreated and treated with the indicated concentrations of edelfosine, were seeded on matrigel-coated culture inserts and allowed to invade and migrate in a gradient of FBS plus insulin for 16 h. Migrated cells were quantified as above (**f**). Magnification, 20x; scale bar, 100 μm. Quantitative results of wound-healing, Boyden chamber and invasion assays are shown. At least three independent experiments were performed in each group. Data are shown as mean ± SD, *$p < 0.05$, **$p < 0.01$, ***$p < 0.001$, ****$p < 0.0001$.

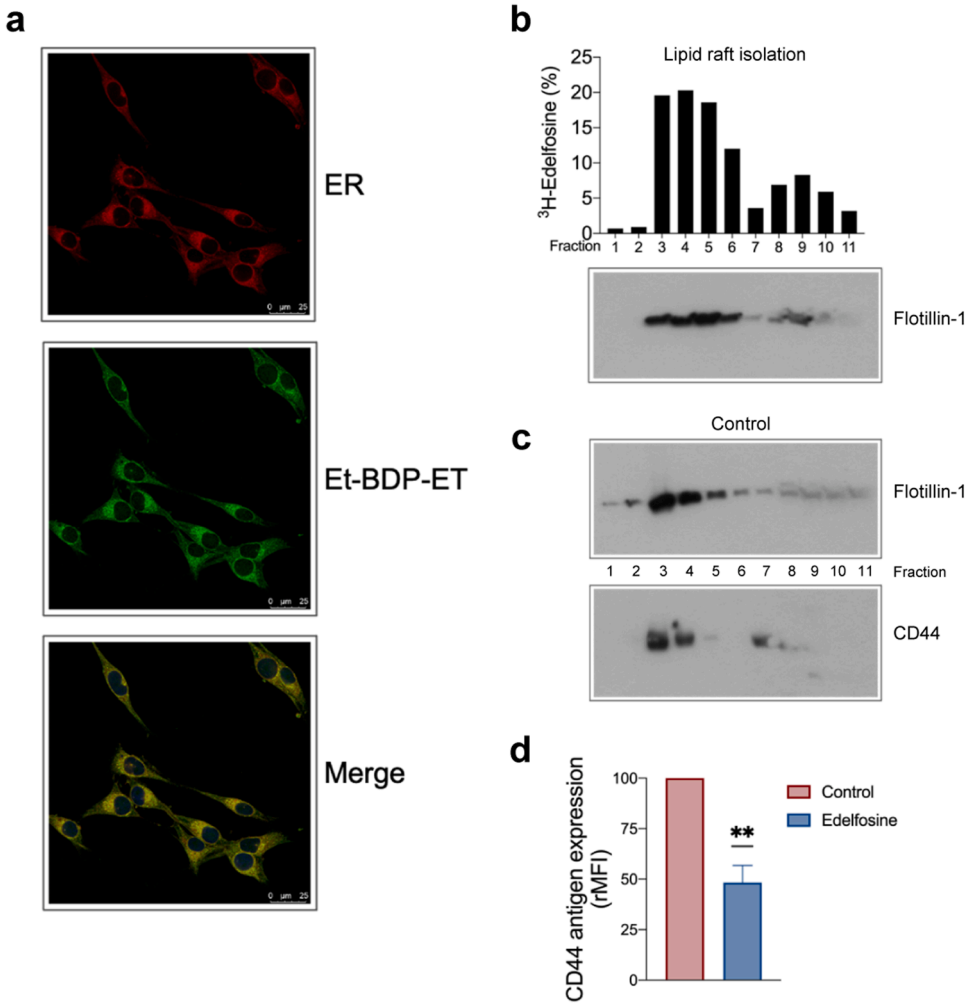

Fig. 6. Subcellular localization of edelfosine in the endoplasmic reticulum and lipid rafts of 435-Lung cells, and down-regulation of raft-located CD44. (**a**) 435-Lung cells were labeled overnight at 37 °C for the endoplasmic reticulum (ER) in red using the Cell Light ER-RFP BacMam 2.0 reagent, and then the samples were incubated with 50 μM Et-BDP-ET (green fluorescence) for 3 h at 37 °C. Areas of colocalization between the ER and Et-BDP-ET in the merge panels are yellow. Scale bar, 25 μm. The data are representative of five independent experiments. (**b**) 435-Lung cells treated with 50 μM [^{3}H]edelfosine for 15 h were lysed in 1% Triton and fractionated by centrifugation on a discontinuous sucrose density gradient for lipid raft isolation as described in the Methods section. An equal volume of each collected fraction was subjected to SDS-PAGE and counted for radioactivity. The distribution patterns of [^{3}H]edelfosine (upper panel) and flotillin-enriched rafts (fractions 3–6) (lower panel) over the gradient fractions are shown. Data are representative of five separate experiments. (**c**) Untreated control 435-Lung cells were lysed in 1% Triton and fractionated by centrifugation on a discontinuous sucrose density gradient for lipid raft isolation as described in the Methods section. An equal volume of each collected fraction was subjected to SDS-PAGE, and the distribution of flotillin-containing rafts (fractions 3–5) and CD44 (fractions 3 and 4) over the gradient fractions is shown. Data are representative of five separate experiments. (**d**) Cell surface expression of CD44 in 435-Lung cells after edelfosine treatment. 435-Lung cells were incubated for 2 days in the absence (*Control*) or in the presence of 50 μM edelfosine (*Edelfosine*). Then, CD44 cell surface expression was analyzed by flow cytometry, and relative mean fluorescence intensity (rMFI) values were estimated using P3×63 myeloma supernatant and an isotype-matched fluorescein isothiocyanate-conjugate nonrelevant IgG monoclonal antibody as negative controls. Cell surface expression (rMFI) of CD44 in untreated control cells was considered as 100. Data shown are means ± SD ($n = 5$). Asterisks denote significant differences with the control group (**, $p < 0.01$). Original uncropped gels of the Western blot results displayed here are shown in Supplementary Fig. S4.

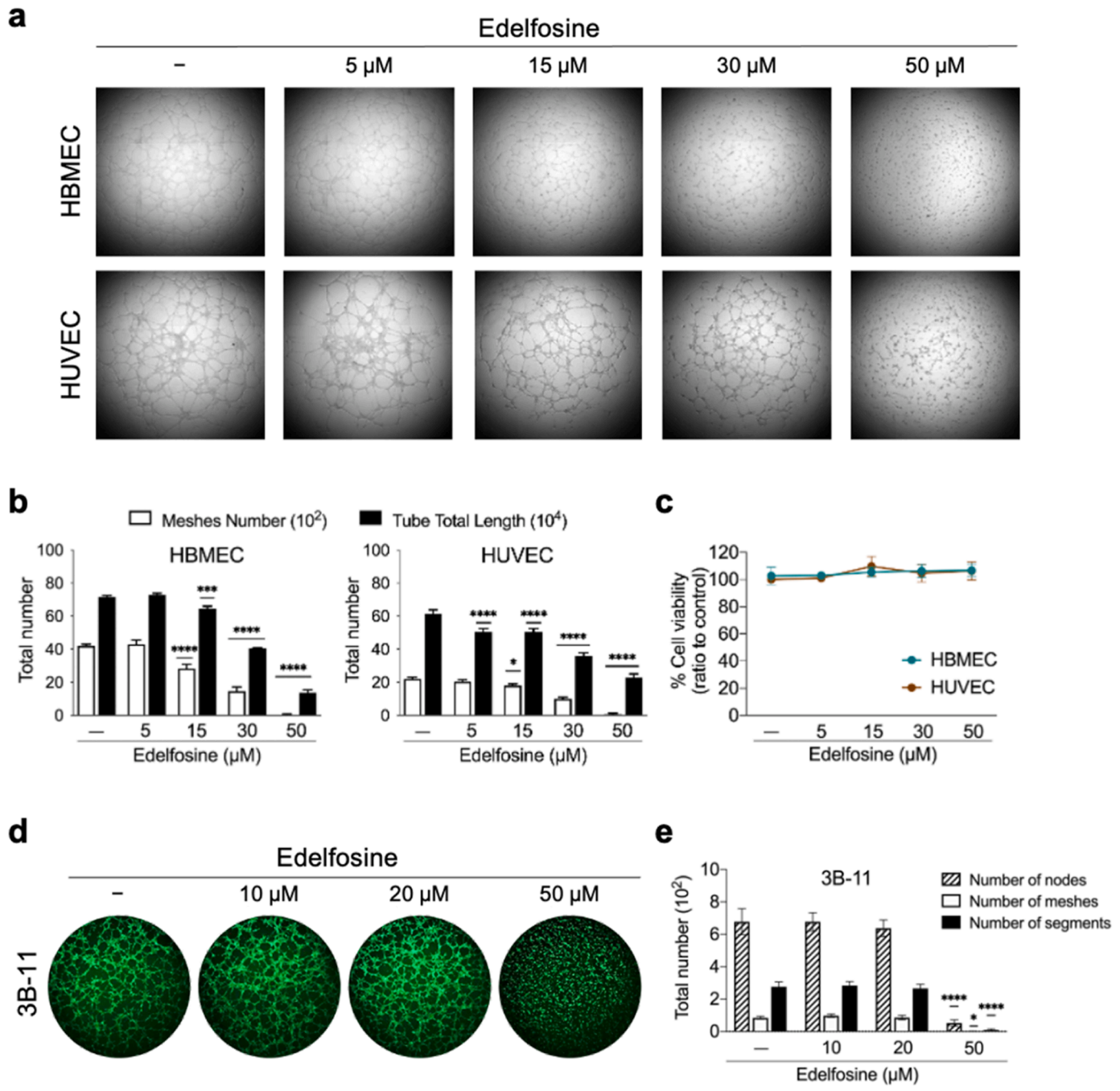

Fig. 7. Edelfosine inhibits angiogenesis in human and mouse models. (**a**) Tube formation assay was performed in HBMEC and HUVEC cells to measure angiogenesis *in vitro*. 2×10^4 cells were seeded in Matrigel-coated 96-well plates, and were untreated or treated with increasing concentrations of edelfosine for 12 h. Tube formation was analyzed using BD Pathway 855 Bioimager (4x). (**b**) Quantification of meshes number and tube total length in HBMEC and HUVEC cells were analyzed using Attovision V 1.7 BD software. Three independent experiments were performed in each group. Data are presented as mean ± SD. * $p < 0.05$, ***$p < 0.001$, **** $p < 0.0001$. (**c**) Metabolically cell viability of HBMEC and HUVEC cells was measured by MTT assay. (**d**) 3B-11 mouse endothelial cells were serum-starved overnight in DMEM with 0.2% FBS, 1% PenStrep, and 1% GlutaMAX, then stained with 2 μg/ml calcein AM for 30 min. 1.8×10^5 cells/well were plated onto basement membrane extract (BME) and exposed to 0 μM, 10 μM, 20 μM, and 50 μM edelfosine in conditioned media. The plates were incubated for 6 h under regular culture conditions and imaged using an Olympus SZX16 dissection scope. (**e**) The tube network was quantified (nodes, meshes, and segments) using ImageJ software as described in the Methods section. Data shown are means ± SD ($n = 5$). Asterisks denote significant differences with the control group (*, $p < 0.05$; ****$p < 0.0001$).

that the effective edelfosine concentration in plasma was reached after approximately 5–6 days of daily oral treatment [69]. Because multiple oral administrations of edelfosine were required to reach a clinically relevant drug plasma concentration, metastatic cells had a period of approximately 10 days to infiltrate and start the process of organ colonization. It is not known precisely how long cancer cells linger in the circulation, but it has been estimated that their dwell time in the bloodstream is rather brief, ranging from minutes to hours, before extravasating into the new tissue [70]. On these grounds, it might be assumed that, in our study, metastatic cells could have reached the target organs as micrometastases or dormant cells before edelfosine action. Thus, edelfosine was likely affecting cancer cells in the early colonization phase. Disseminated cancer cells must overcome many obstacles and survive at the new distant tissue as latent tumor-initiating

seeds, which eventually break out to replace the host tissue [4]. Lipid rafts play an important role in many survival pathways in cancer cells [12], and the impairment of these signaling routes could have an impact on their capacity to survive and proliferate in the new microenvironment. Edelfosine has been shown to target lipid rafts on cancer cells, leading to their own cell demise, and this lipid raft-targeted ether lipid is effective in causing tumor cell death in both *in vitro* and *in vivo* models [17,18,29]. Here, we found that edelfosine accumulated in lipid rafts in metastatic cells, raising the possibility that the lipid raft-mediated action of edelfosine against cancer cells might affect metastatic cell dissemination and survival after organ colonization.

The 435-Lung cell line is a variant of the MDA-MB-435 cell line that has been previously used for metastatic studies [44]. MDA-MB-435 cell line, originally derived from pleural effusion of a female breast cancer patient in 1976 at MD Anderson, Houston, TX, USA, has mistakenly been used as a model for human breast cancer for a long time [71]. However, despite controversy [72], a number of molecular studies, including gene expression, SNP arrays, miRNA expression, and CpG island promoter hypermethylation, have determined that the MDA-MB-435 cells are of melanoma origin [71,73]. Malignant melanoma is one of the most aggressive cancers and can disseminate and metastasize to multiple sites, including the lung (18–36%), brain (12–20%), liver (14–20%), and bone (11–17%) [74]. Brain metastases from different cancer types, such as melanoma, breast cancer, and lung cancer, are approximately ten times more prevalent than primary central nervous system tumors in adults, and often herald advanced cancer stages due to limited effective treatments [75]. Chemotherapeutic delivery to brain neoplasms is hampered by the presence of the blood-brain barrier (BBB), formed by specialized brain microvascular endothelial cells and surrounded by other cells of the neurovascular unit, including astrocytes, pericytes, and neurons. The inability for some drugs to cross the BBB is one of the main barriers to the effective treatment of brain metastasis [76]. Interestingly, the results herein reported, showing that edelfosine completely inhibits brain colonization by cancer cells, are especially relevant because there is a lack of effective treatments for brain metastases and prognosis is very poor. Previous biodistribution studies using orally administered free edelfosine revealed that the drug was widely scattered in many organs, but only a small amount was found in the brain [69]. However, the integrity of the BBB is altered in both primary and metastatic brain tumors, becoming more permeable [77]. In our experimental model, cancer cells were expected to be localized to a novel metastatic colonization site, such as brain, by the time mice started to be orally treated with edelfosine. Thus, our results suggest that edelfosine could cross the BBB and block tumor proliferation. In addition, because edelfosine has been shown, both *in vitro* and *in vivo*, to accumulate in the tumor tissue and induce apoptosis selectively in tumor cells [17,18,22,23,29,31], it is tempting to envisage that the ether lipid edelfosine could accrue in the novel and distant metastatic colonization site, and once there, after reaching a threshold concentration, it would induce cancer cell apoptosis. On the other hand, it is worth noting that oral administration of edelfosine in lipid nanoparticles [78] increases its accumulation in brain [79]. Taken together, these data suggest that edelfosine could be a promising drug for the prevention and treatment of brain metastasis.

In addition, we have found here that edelfosine inhibited cancer cell adhesion to collagen-I and laminin-I coated plates, as well as cell migration of cancer cells. Importantly, edelfosine accumulates in lipid rafts and endoplasmic reticulum of metastatic 435-Lung cells, in agreement with previous reports using distinct tumor cells [18,23,25,30,31,34,37] and yeast [36], leading to lipid raft reorganization [20,23,25,31,36,80]. Because the endoplasmic reticulum interacts with the mitochondria through cholesterol-rich platforms named as mitochondria-associated membranes (MAMs), we have recently envisaged that edelfosine could target these raft-mediated membrane–endoplasmic reticulum–mitochondria networks that could modulate cell fate [37]. In this regard, it is interesting to note that edelfosine has also been located in mitochondria in cancer cells [48] and *Leishmania* parasites [81], and lipid rafts have also been involved in this subcellular location [81]. Although the data reported here and in previous studies [18,31] show a certain percentage of edelfosine in other non-raft fractions, most of the ether lipid accumulates in the lipid raft membrane domains. In this context, it is worth keeping in mind that biophysical approaches have shown that edelfosine has a high affinity for cholesterol and alters liquid-ordered membrane structures [82]. Interestingly, studies in *S. cerevisiae* yeast cells have shown that edelfosine was mainly located in non-raft fractions at very early incubation times, but it accumulated in rafts at longer incubation times [36], leading to a selective modification of lipid raft composition [36,83,84].

The ether lipid edelfosine has been reported to abrogate neutrophil adhesion to the endothelium through L-selectin shedding [28], and to downregulate cell surface expression of CD43 and CD44 adhesion molecules in human peripheral blood neutrophils [28]. Interestingly, L-selectin [85] as well as CD44 [86] have been found to be located in lipid rafts. Here, we found that CD44, which has been involved in metastasis [12,65], is present in the lipid raft fraction of resting 435-Lung cells and is downregulated upon edelfosine treatment. Since edelfosine accumulates in lipid rafts, it is possible that lipid raft reorganization induced by edelfosine could underlie most of its effects on cell adhesion and migration. Therefore, the inhibitory effect of edelfosine on cancer cell adhesion and migration could account for its efficient antimetastatic action, which, in turn, might be related to its targeting to lipid rafts. In addition, edelfosine and its lactose-based ether lipid analog named ohmline have also been found to block the potassium channel SK3, leading to a decrease in tumor cell migration [59,87]. The activity of the SK3 channel, abnormally expressed in melanoma and breast tumor cells [88,89], is dependent on its lipid raft location [90], and the SK3 channel has shown to be a target for edelfosine [59]. Thus, it has been postulated that lipid raft reorganization by edelfosine or ohmline might move the SK3 channel away from lipid rafts inhibiting its activity as well as cell migration and metastasis [91].

Edelfosine also inhibited tube formation of human umbilical vein endothelial cells (HUVECs), human brain microvascular endothelial cells (HBMECs), and 3B-11 mouse endothelial cells, without affecting their cell viability, thus strongly suggesting that this ether lipid inhibits angiogenesis. This agrees with previous reports showing an antiangiogenic effect of edelfosine by using a human microvascular endothelial cell line (HMEC-1) [92], and the inability to mount a corneal neovascular response to a pellet releasing the angiogenic basic fibroblastic growth factor in edelfosine-treated rats [93]. Edelfosine required rather high concentrations to inhibit angiogenesis. We have previously found in pharmacokinetic and biodistribution studies that the plasma concentration of edelfosine in drug-treated mice ranges between 10 and 23 μM [18,29,69], but edelfosine was remarkably concentrated in the tumor after a daily oral administration dose of 30 mg/kg edelfosine in tumor-bearing mice for several weeks, reaching over 16-fold higher drug concentration in the tumor as compared to the plasma level [18,29]. This indicates a preferential tumor location for this ether lipid, in agreement with the selective edelfosine uptake in tumor cells [22,54,94,95]. Thus, due to the edelfosine accumulation in the tumor, a high concentration of edelfosine can be reached at the tumor site and possibly adjacent areas, inhibiting angiogenesis and eventually inducing cancer cell death. This *in vivo* and *in vitro* selectivity of edelfosine for malignant cells, sparing normal cells, could explain the herein reported lack of weight loss and the absence of any histologically adverse effect in mice after drug treatment, in agreement with the apparent lack of toxicity of this ether lipid in different *in vivo* settings following organ examination at necropsy [18,29,30,33,35]. Furthermore, the amphiphilic molecule edelfosine inserts readily into lipid monolayers and bilayers but displays a low detergent activity [58], and its pro-apoptotic activity is highly dependent on its molecular structure [22,57]. In this regard, closely structurally related inactive analogs did not induce cell death even at concentrations of 50 and 75 μM.

Fig. 8 summarizes the results herein reported and depicts the

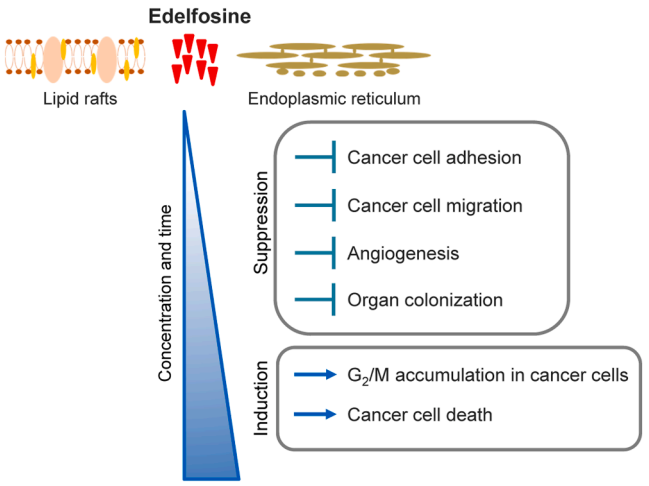

Fig. 8. Schematic model for the suppression of metastatic organ colonization by edelfosine in cancer. This is a schematic diagram designed to portray one plausible mechanism for how edelfosine inhibits cancer metastasis. Edelfosine is incorporated into the tumor cell and accumulates in membrane rafts and the endoplasmic reticulum, inhibiting cancer cell adhesion and migration, metastatic organ colonization and angiogenesis in a concentration- and time-dependent manner. At high drug concentrations, which can be achieved at the tumor site, G_2/M accumulation of cancer cells and subsequent cell death may occur. See text for details.

manifold effects of oral administration of edelfosine on various processes involved in metastatic organ colonization. Taken into account the timing and drug concentrations required to show those diverse effects, it is plausible to propose that edelfosine affects different metastasis-related processes in a dose- and time-dependent manner, eventually leading to the demise of cancer cells (Fig. 8).

An outstanding feature of at least some APLs, including edelfosine, lie in their selectivity for tumor cells [18,22,25,29,96,97]. The ether lipid edelfosine is selectively taken up by different tumor cells, which subsequently undergo apoptosis, while normal untransformed cells do not incorporate significant drug amounts and are spared [22,23,25,31,54]. The underlying mechanism for this selective uptake remains to be elucidated, but several items seem to be involved in APL uptake, such as: an intact cholesterol-rich lipid raft organization [18,29]; the expression of *LEM3, AGP2,* and *DOC1* in yeast [36]; the transmembrane protein 30A (TMEM30A; a.k.a. CDC50A) [98], which enables phospholipid flippase activity. On the other hand, it is worth noting that naturally occurring phospholipid ethers selectively accumulate in human cancers compared to normal cells [99]. This selectivity for different tumor cells, without affecting normal cells, suggests that APLs could act as promising antitumor drugs with wide-range tumor theranostic (diagnostic and therapeutic) abilities. They can be used for direct tumor imaging and therapy as well as a cancer drug delivery vehicle with broad-spectrum applicability, as compared to more narrowly targeted delivery mechanisms. In addition, APLs do not interact with DNA while inducing apoptosis, further minimizing damage to normal cells [91,94–96].

Edelfosine has been shown to be effective against primary tumor cells derived from hematological cancer patients and solid tumor patients [18,22,25,29,34]. Moreover, the rather unique mechanism of action of edelfosine makes it well suited for combination therapy regimens [33–35,100]. Edelfosine as well as other APLs have also been reported to enhance the cytotoxic effect of radiation in preclinical models, making these compounds attractive candidates as clinical radiosensitizers in cancer radiotherapy [101,102]. Furthermore, the use of edelfosine-loaded solid lipid nanoparticles also potentiates the *in vivo* antitumor action of the ether lipid [79,103].

Edelfosine is not toxic to normal cells at concentrations that kill a broad range of tumor cells, and it can be orally given over a long period safely in animal tests. It has no significant toxicity or systemic side effects, no bone marrow toxicity, no mutagenic or cytogenetic effects, and the main side effect being gastrointestinal irritation is manageable [28,94]. The results reported here indicate that the ether lipid edelfosine displays potent activity against metastatic colonization and angiogenesis, two major and clinically relevant features of tumor malignancy. These results warrant further research to explore the underlying mechanisms involved in the effect of this APL to block and prevent metastasis. Thus, edelfosine could be a strong candidate for improving the landscape of cancer therapy, both for the selective killing of tumor cells and for the prevention of cancer metastasis to various organs. Because of its broad-spectrum applicability in different tumors, it represents an improvement over other more narrowly targeted therapies. In addition, our results further suggest that lipid rafts could represent a vulnerability in tumor cells that can be exploited for targeted cancer therapy. Importantly, because edelfosine was the first lipid raft-targeted antitumor drug, this ether lipid could be used as a probe to further analyze the involvement and role of lipid raft-mediated processes in metastasis and tumor development.

5. Conclusions

This study shows that edelfosine oral administration prevents brain and lung colonization of cancer cells. Edelfosine also inhibits different steps involved in metastasis, including cancer cell adhesion and migration as well as cancer cell invasion. Edelfosine accumulates in lipid rafts, and prevents metastatic organ colonization and angiogenesis, two major and relevant hallmarks of tumor malignancy. Thus, these data provide a preclinical rationale to further evaluate this orally administered raft-targeted drug edelfosine as a promising antitumor agent, and might support the involvement of lipid rafts in cancer metastasis.

Ethics approval and consent to participate

All animal-related procedures were performed in accordance with the National Institute of Health guidelines for the Care and Use of Laboratory Animals, with the approval of the animal care committee (reference 9703). The IDIBELL Animal Care Facility Committee approved all animal studies.

Funding

This work was supported by grants PID2020–119656RB-I00 (to FM) and PID2021–124314OB-I00 (to MAC) funded by MCIN/AEI/10.13039/501100011033 from the Spanish Ministry of Science and Innovation (Agencia Estatal de Investigación), as well as by grants from the Spanish Ministry of Science, Innovation and Universities and Ministry of Economy and Competitiveness (SAF2017–89672-R, SAF2014–59716-R, and SAF2008–02251) (to FM), Spanish Ministry of Health and Consumer Affairs, the ISCIII-Subdirección General de Evaluación and the Fondo Europeo de Desarrollo Regional (FEDER) – FIS-PI14/00336 and FIS-PI18/00916 (to AS), Generalitat de Catalunya and Fundació Privada Cellex Barcelona (2014 SGR 530) (to AS), Conserjería de Salud of the Junta de Andalucía (PI-0246–2013) (to MAC), RD06/0020/1037 and RD12/0036/0065 from Red Temática de Investigación Cooperativa en Cáncer-Instituto de Salud Carlos III (RTICC-ISCIII), cofunded by the EU's European Regional Development Fund – FEDER (to FM), and European Community's Seventh Framework Program FP7–2007-2013 (grant HEALTH-F2–2011-256986) (to FM). V.A.-P. acknowledges a predoctoral project-based fellowship from the Ministry of Science and Innovation (BES-2009–024462), and a short-term fellowship from the RTICC-ISCIII. AV-B. acknowledges a predoctoral fellowship from the Ministry of Education, Culture and Sport of Spain (FPU2015/02457) and a short-term EST18/00016 fellowship (Ayuda FPU para Estancias Breves) from the Ministry of Education, Culture and Sport of Spain. F.M. belongs to the Spanish National Research Council (CSIC)'s Cancer Hub.

CRediT authorship contribution statement

Gajate Consuelo: Data curation, Formal analysis, Investigation, Methodology, Visualization, Writing – review & editing. **Soler-Torronteras Rafael:** Formal analysis, Investigation, Methodology. **Calzado Marco A.:** Data curation, Formal analysis, Funding acquisition, Investigation, Methodology, Visualization, Writing – review & editing. **Vicente-Blázquez Alba:** Data curation, Formal analysis, Investigation, Methodology, Visualization, Writing – review & editing. **Mollinedo Faustino:** Conceptualization, Data curation, Formal analysis, Funding acquisition, Investigation, Methodology, Project administration, Supervision, Visualization, Writing – original draft, Writing – review & editing. **DeCicco-Skinner Kathleen:** Data curation, Formal analysis, Investigation, Methodology, Visualization, Writing – review & editing. **Sierra Angels:** Data curation, Formal analysis, Funding acquisition, Investigation, Methodology, Visualization, Writing – review & editing. **Hernández Vanessa:** Formal analysis, Investigation, Methodology. **Alonso-Pérez Verónica:** Conceptualization, Data curation, Formal analysis, Investigation, Methodology, Visualization, Writing – review & editing.

Declaration of Competing Interest

The authors declare no competing interests.

Acknowledgments

We are grateful to María del Carmen García Macías (IBMCC, Salamanca, Spain) for her help in the histological studies.

Appendix A. Supporting information

Supplementary data associated with this article can be found in the online version at doi:10.1016/j.biopha.2024.116149.

References

[1] H. Dillekas, M.S. Rogers, O. Straume, Are 90% of deaths from cancer caused by metastases? Cancer Med. 8 (2019) 5574–5576.
[2] J. Fares, M.Y. Fares, H.H. Khachfe, H.A. Salhab, Y. Fares, Molecular principles of metastasis: a hallmark of cancer revisited, Signal Transduct. Target Ther. 5 (2020) 28.
[3] M. Riihimaki, H. Thomsen, A. Hemminki, K. Sundquist, K. Hemminki, Comparison of survival of patients with metastases from known versus unknown primaries: survival in metastatic cancer, BMC Cancer 13 (2013) 36.
[4] J. Massague, A.C. Obenauf, Metastatic colonization by circulating tumour cells, Nature 529 (2016) 298–306.
[5] F. Mollinedo, Neutrophil degranulation, plasticity, and cancer metastasis, Trends Immunol. 40 (2019) 228–242.
[6] A. Kogure, N. Kosaka, T. Ochiya, Cross-talk between cancer cells and their neighbors via mirna in extracellular vesicles: an emerging player in cancer metastasis, J. Biomed. Sci. 26 (2019) 7.
[7] D. Hanahan, R.A. Weinberg, Hallmarks of cancer: the next generation, Cell 144 (2011) 646–674.
[8] P.S. Steeg, D. Theodorescu, Metastasis: a therapeutic target for cancer, Nat. Clin. Pract. Oncol. 5 (2008) 206–219.
[9] K. Ganesh, J. Massague, Targeting metastatic cancer, Nat. Med. 27 (2021) 34–44.
[10] A.C. Obenauf, J. Massague, Surviving at a distance: Organ specific metastasis, Trends Cancer 1 (2015) 76–91.
[11] T. Murai, The role of lipid rafts in cancer cell adhesion and migration, Int. J. Cell Biol. 2012 (2012) 763283.
[12] F. Mollinedo, C. Gajate, Lipid rafts as signaling hubs in cancer cell survival/death and invasion: implications in tumor progression and therapy, J. Lipid Res. 61 (2020) 611–635.
[13] X. Luo, C. Cheng, Z. Tan, N. Li, M. Tang, L. Yang, Y. Cao, Emerging roles of lipid metabolism in cancer metastasis, Mol. Cancer 16 (2017) 76.
[14] V.K. Gupta, N.S. Sharma, K. Kesh, P. Dauer, A. Nomura, B. Giri, V. Dudeja, S. Banerjee, S. Bhattacharya, A. Saluja, S. Banerjee, Metastasis and chemoresistance in CD133 expressing pancreatic cancer cells are dependent on their lipid raft integrity, Cancer Lett. 439 (2018) 101–112.
[15] J.D. Greenlee, T. Subramanian, K. Liu, M.R. King, Rafting down the metastatic cascade: the role of lipid rafts in cancer metastasis, cell death, and clinical outcomes, Cancer Res. 81 (2021) 5–17.
[16] C. Gajate, F. Mollinedo, The antitumor ether lipid ET-18-OCH_3 induces apoptosis through translocation and capping of Fas/CD95 into membrane rafts in human leukemic cells, Blood 98 (2001) 3860–3863.
[17] F. Mollinedo, C. Gajate, Fas/CD95 death receptor and lipid rafts: new targets for apoptosis-directed cancer therapy, Drug Resist Updat 9 (2006) 51–73.
[18] F. Mollinedo, J. de la Iglesia-Vicente, C. Gajate, A. Estella-Hermoso de Mendoza, J.A. Villa-Pulgarin, M.A. Campanero, M.J. Blanco-Prieto, Lipid raft-targeted therapy in multiple myeloma, Oncogene 29 (2010) 3748–3757.
[19] F. Mollinedo, C. Gajate, Lipid rafts and clusters of apoptotic signaling molecule-enriched rafts in cancer therapy, Future Oncol. 6 (2010) 811–821.
[20] C. Gajate, F. Mollinedo, Lipid raft-mediated Fas/CD95 apoptotic signaling in leukemic cells and normal leukocytes and therapeutic implications, J. Leukoc. Biol. 98 (2015) 739–759.
[21] C. Gajate, F. Mollinedo, Lipid rafts and raft-mediated supramolecular entities in the regulation of CD95 death receptor apoptotic signaling, Apoptosis 20 (2015) 584–606.
[22] F. Mollinedo, J.L. Fernandez-Luna, C. Gajate, B. Martin-Martin, A. Benito, R. Martinez-Dalmau, M. Modolell, Selective induction of apoptosis in cancer cells by the ether lipid ET-18-OCH_3 (Edelfosine): molecular structure requirements, cellular uptake, and protection by Bcl-2 and Bcl-X_L, Cancer Res. 57 (1997) 1320–1328.
[23] C. Gajate, E. Del Canto-Janez, A.U. Acuña, F. Amat-Guerri, E. Geijo, A.M. Santos-Beneit, R.J. Veldman, F. Mollinedo, Intracellular triggering of Fas aggregation and recruitment of apoptotic molecules into Fas-enriched rafts in selective tumor cell apoptosis, J. Exp. Med. 200 (2004) 353–365.
[24] M. Reis-Sobreiro, G. Roue, A. Moros, C. Gajate, J. de la Iglesia-Vicente, D. Colomer, F. Mollinedo, Lipid raft-mediated AKT signaling as a therapeutic target in mantle cell lymphoma, Blood Cancer J. 3 (2013) e118.
[25] C. Gajate, F. Mollinedo, Edelfosine and perifosine induce selective apoptosis in multiple myeloma by recruitment of death receptors and downstream signaling molecules into lipid rafts, Blood 109 (2007) 711–719.
[26] S. Melo-Lima, C. Gajate, F. Mollinedo, Triggers and signaling cross-talk controlling cell death commitment, Cell Cycle 14 (2015) 465–466.
[27] S. Melo-Lima, M.C. Lopes, F. Mollinedo, ERK1/2 acts as a switch between necrotic and apoptotic cell death in ether phospholipid edelfosine-treated glioblastoma cells, Pharm. Res. 95-96C (2015) 2–11.
[28] F. Mollinedo, C. Gajate, A.I. Morales, E. del Canto-Janez, N. Justies, F. Collia, J. V. Rivas, M. Modolell, A. Iglesias, Novel anti-inflammatory action of edelfosine lacking toxicity with protective effect in experimental colitis, J. Pharmacol. Exp. Ther. 329 (2009) 439–449.
[29] F. Mollinedo, J. de la Iglesia-Vicente, C. Gajate, A. Estella-Hermoso de Mendoza, J.A. Villa-Pulgarin, M. de Frias, G. Roue, J. Gil, D. Colomer, M.A. Campanero, M. J. Blanco-Prieto, *In vitro* and *in vivo* selective antitumor activity of edelfosine against mantle cell lymphoma and chronic lymphocytic leukemia involving lipid rafts, Clin. Cancer Res. 16 (2010) 2046–2054.
[30] C. Gajate, M. Matos-da-Silva, E.L. Dakir, R.I. Fonteriz, J. Alvarez, F. Mollinedo, Antitumor alkyl-lysophospholipid analog edelfosine induces apoptosis in pancreatic cancer by targeting endoplasmic reticulum, Oncogene 31 (2012) 2627–2639.
[31] C. Gajate, F. Gonzalez-Camacho, F. Mollinedo, Involvement of raft aggregates enriched in Fas/CD95 death-inducing signaling complex in the antileukemic action of edelfosine in jurkat cells, PLOS One 4 (2009) e5044.
[32] T. Nieto-Miguel, C. Gajate, F. Mollinedo, Differential targets and subcellular localization of antitumor alkyl-lysophospholipid in leukemic *versus* solid tumor cells, J. Biol. Chem. 281 (2006) 14833–14840.
[33] X. Bonilla, H. Dakir el, F. Mollinedo, C. Gajate, Endoplasmic reticulum targeting in Ewing's sarcoma by the alkylphospholipid analog edelfosine, Oncotarget 6 (2015) 14596–14613.
[34] C. Gajate, O. Gayet, N.A. Fraunhoffer, J. Iovanna, N. Dusetti, F. Mollinedo, Induction of apoptosis in human pancreatic cancer stem cells by the endoplasmic reticulum-targeted alkylphospholipid analog edelfosine and potentiation by autophagy inhibition, Cancers 13 (2021) 6124.
[35] E.H. Dakir, C. Gajate, F. Mollinedo, Antitumor activity of alkylphospholipid edelfosine in prostate cancer models and endoplasmic reticulum targeting, Biomed. Pharmacother. 167 (2023) 115436.
[36] A. Cuesta-Marban, J. Botet, O. Czyz, L.M. Cacharro, C. Gajate, V. Hornillos, J. Delgado, H. Zhang, F. Amat-Guerri, A.U. Acuña, C.R. McMaster, J.L. Revuelta, V. Zaremberg, F. Mollinedo, Drug uptake, lipid rafts, and vesicle trafficking modulate resistance to an anticancer lysophosphatidylcholine analogue in yeast, J. Biol. Chem. 288 (2013) 8405–8418.
[37] F. Mollinedo, C. Gajate, Direct endoplasmic reticulum targeting by the selective alkylphospholipid analog and antitumor ether lipid edelfosine as a therapeutic approach in pancreatic cancer, Cancers 13 (2021) 4173.
[38] C. Gajate, F. Mollinedo, Lipid rafts, endoplasmic reticulum and mitochondria in the antitumor action of the alkylphospholipid analog edelfosine, Anticancer Agents Med. Chem. 14 (2014) 509–527.
[39] A. Burgeiro, C.V. Pereira, F.S. Carvalho, G.C. Pereira, F. Mollinedo, P.J. Oliveira, Edelfosine and perifosine disrupt hepatic mitochondrial oxidative phosphorylation and induce the permeability transition, Mitochondrion 13 (2013) 25–35.
[40] A. Sanchez-Blanco, A.G. Rodriguez-Matellan, M. Reis-Sobreiro, B. Saenz-Narciso, J. Cabello, W.A. Mohler, F. Mollinedo, *Caenorhabditis elegans* as a platform to study the mechanism of action of synthetic antitumor lipids, Cell Cycle 13 (2014) 3375–3389.

[41] O. Mendez, Y. Fernandez, M.A. Peinado, V. Moreno, A. Sierra, Anti-apoptotic proteins induce non-random genetic alterations that result in selecting breast cancer metastatic cells, Clin. Exp. Metastas. 22 (2005) 297–307.

[42] E.A. Clark, T.R. Golub, E.S. Lander, R.O. Hynes, Genomic analysis of metastasis reveals an essential role for Rhoc, Nature 406 (2000) 532–535.

[43] R. Sanz, R. Arragues, V. Stresing, B. Martin, T. Landemaine, B. Oliva, K. Driouch, R. Lidereau, A. Sierra, Functional pathways shared by liver and lung metastases: A mitochondrial chaperone machine is up-regulated in soft-tissue breast cancer metastasis, Clin. Exp. Metastas. 24 (2007) 673–683.

[44] Y. Kienast, L. von Baumgarten, M. Fuhrmann, W.E. Klinkert, R. Goldbrunner, J. Herms, F. Winkler, Real-time imaging reveals the single steps of brain metastasis formation, Nat. Med. 16 (2010) 116–122.

[45] V. Stresing, E. Baltziskueta, N. Rubio, J. Blanco, M.C. Arriba, J. Valls, M. Janier, P. Clezardin, R. Sanz-Pamplona, C. Nieva, M. Marro, D. Petrov, A. Sierra, Peroxiredoxin 2 specifically regulates the oxidative and metabolic stress response of human metastatic breast cancer cells in lungs, Oncogene 32 (2013) 724–735.

[46] I. Roman, M. Vilalta, J. Rodriguez, A.M. Matthies, S. Srouji, E. Livne, J. A. Hubbell, N. Rubio, J. Blanco, Analysis of progenitor cell-scaffold combinations by *in vivo* non-invasive photonic imaging, Biomaterials 28 (2007) 2718–2728.

[47] C. Gajate, A.M. Santos-Beneit, A. Macho, M. Lazaro, A. Hernandez-De Rojas, M. Modolell, E. Muñoz, F. Mollinedo, Involvement of mitochondria and caspase-3 in ET-18-OCH_3-induced apoptosis of human leukemic cells, Int. J. Cancer 86 (2000) 208–218.

[48] F. Mollinedo, M. Fernandez, V. Hornillos, J. Delgado, F. Amat-Guerri, A.U. Acuña, T. Nieto-Miguel, J.A. Villa-Pulgarin, C. Gonzalez-Garcia, V. Cena, C. Gajate, Involvement of lipid rafts in the localization and dysfunction effect of the antitumor ether phospholipid edelfosine in mitochondria, Cell Death Dis. 2 (2011) e158.

[49] C. Gajate, F. Mollinedo, Lipid raft isolation by sucrose gradient centrifugation and visualization of raft-located proteins by fluorescence microscopy: The use of combined techniques to assess Fas/CD95 location in rafts during apoptosis triggering, Methods Mol. Biol. 2187 (2021) 147–186.

[50] C. Gajate, F. Mollinedo, Isolation of lipid rafts through discontinuous sucrose gradient centrifugation and Fas/CD95 death receptor localization in raft fractions, Methods Mol. Biol. 1557 (2017) 125–138.

[51] H. Yokoyama, I. Matsui, The lipid raft markers stomatin, prohibitin, flotillin, and HflK/C (SPFH)-domain proteins form an operon with NfeD proteins and function with apolar polyisoprenoid lipids, Crit. Rev. Microbiol. 46 (2020) 38–48.

[52] M. Kelley, S. Fierstein, L. Purkey, K. DeCicco-Skinner, Endothelial cell tube formation assay: an *in vitro* model for angiogenesis, Methods Mol. Biol. 2475 (2022) 187–196.

[53] W.E. Damsky, L.E. Rosenbaum, M. Bosenberg, Decoding melanoma metastasis, Cancers 3 (2010) 126–163.

[54] C. Gajate, R.I. Fonteriz, C. Cabaner, G. Alvarez-Noves, Y. Alvarez-Rodriguez, M. Modolell, F. Mollinedo, Intracellular triggering of Fas, independently of Fasl, as a new mechanism of antitumor ether lipid-induced apoptosis, Int. J. Cancer 85 (2000) 674–682.

[55] T. Nieto-Miguel, R.I. Fonteriz, L. Vay, C. Gajate, S. Lopez-Hernandez, F. Mollinedo, Endoplasmic reticulum stress in the proapoptotic action of edelfosine in solid tumor cells, Cancer Res. 67 (2007) 10368–10378.

[56] N. Santana-Codina, A. Marce-Grau, L. Muixi, C. Nieva, M. Marro, D. Sebastian, J. P. Munoz, A. Zorzano, A. Sierra, GRP94 is involved in the lipid phenotype of brain metastatic cells, Int. J. Mol. Sci. 20 (2019) 3883.

[57] C. Gajate, A. Santos-Beneit, M. Modolell, F. Mollinedo, Involvement of c-*jun* NH_2-terminal kinase activation and c-*jun* in the induction of apoptosis by the ether phospholipid 1-*O*-octadecyl-2-*O*-methyl-*rac*-glycero-3-phosphocholine, Mol. Pharmacol. 53 (1998) 602–612.

[58] J.V. Busto, J. Sot, F.M. Goni, F. Mollinedo, A. Alonso, Surface-active properties of the antitumour ether lipid 1-*O*-octadecyl-2-*O*-methyl-*rac*-glycero-3-phosphocholine (edelfosine), Biochim. Biophys. Acta 1768 (2007) 1855–1860.

[59] M. Potier, A. Chantome, V. Joulin, A. Girault, S. Roger, P. Besson, M.L. Jourdan, J.Y. LeGuennec, P. Bougnoux, C. Vandier, The SK3/K_{Ca}2.3 potassium channel is a new cellular target for edelfosine, Br. J. Pharmacol. 162 (2011) 464–479.

[60] D. Korentzelos, A.M. Clark, A. Wells, A perspective on therapeutic pan-resistance in metastatic cancer, Int. J. Mol. Sci. 21 (2020).

[61] S.Y. Park, J.S. Nam, The force awakens: metastatic dormant cancer cells, Exp. Mol. Med. 52 (2020) 569–581.

[62] N.K. Karamanos, A.D. Theocharis, Z. Piperigkou, D. Manou, A. Passi, S. S. Skandalis, D.H. Vynios, V. Orian-Rousseau, S. Ricard-Blum, C.E.H. Schmelzer, L. Duca, M. Durbeej, N.A. Afratis, L. Troeberg, M. Franchi, V. Masola, M. Onisto, A guide to the composition and functions of the extracellular matrix, FEBS J. 288 (2021) 6850–6912.

[63] Y.L. Liu, C.K. Chou, M. Kim, R. Vasisht, Y.A. Kuo, P. Ang, C. Liu, E.P. Perillo, Y. A. Chen, K. Blocher, H. Horng, Y.I. Chen, D.T. Nguyen, T.E. Yankeelov, M. C. Hung, A.K. Dunn, H.C. Yeh, Assessing metastatic potential of breast cancer cells based on EGFR dynamics, Sci. Rep. 9 (2019) 3395.

[64] R. Cailleau, M. Olive, Q.V. Cruciger, Long-term human breast carcinoma cell lines of metastatic origin: preliminary characterization, Vitro 14 (1978) 911–915.

[65] C. Chen, S. Zhao, A. Karnad, J.W. Freeman, The biology and role of CD44 in cancer progression: therapeutic implications, J. Hematol. Oncol. 11 (2018) 64.

[66] P. Mehlen, A. Puisieux, Metastasis: a question of life or death, Nat. Rev. Cancer 6 (2006) 449–458.

[67] W. Liu, B. Chakraborty, R. Safi, D. Kazmin, C.Y. Chang, D.P. McDonnell, Dysregulated cholesterol homeostasis results in resistance to ferroptosis increasing tumorigenicity and metastasis in cancer, Nat. Commun. 12 (2021) 5103.

[68] J. Nakayama, Y. Han, Y. Kuroiwa, K. Azuma, Y. Yamamoto, K. Semba, The *in vivo* selection method in breast cancer metastasis, Int. J. Mol. Sci. 22 (2021) 1886.

[69] A. Estella-Hermoso de Mendoza, M.A. Campanero, J. de la Iglesia-Vicente, C. Gajate, F. Mollinedo, M.J. Blanco-Prieto, Antitumor alkyl ether lipid edelfosine: tissue distribution and pharmacokinetic behavior in healthy and tumor-bearing immunosuppressed mice, Clin. Cancer Res. 15 (2009) 858–864.

[70] S. Valastyan, R.A. Weinberg, Tumor metastasis: molecular insights and evolving paradigms, Cell 147 (2011) 275–292.

[71] V.V. Prasad, R.O. Gopalan, Continued use of MDA-MB-435, a melanoma cell line, as a model for human breast cancer, even in year, 2014, NPJ Breast Cancer 1 (2015) 15002.

[72] A.F. Chambers, MDA-MB-435 and M14 cell lines: identical but not M14 melanoma? Cancer Res. 69 (2009) 5292–5293.

[73] J.M. Rae, C.J. Creighton, J.M. Meck, B.R. Haddad, M.D. Johnson, MDA-MB-435 cells are derived from M14 melanoma cells–a loss for breast cancer, but a boon for melanoma research, Breast Cancer Res. Treat. 104 (2007) 13–19.

[74] F. Tas, Metastatic behavior in melanoma: Timing, pattern, survival, and influencing factors, J. Oncol. 2012 (2012) 647684.

[75] S. Puhalla, W. Elmquist, D. Freyer, L. Kleinberg, C. Adkins, P. Lockman, J. McGregor, L. Muldoon, G. Nesbit, D. Peereboom, Q. Smith, S. Walker, E. Neuwelt, Unsanctifying the sanctuary: challenges and opportunities with brain metastases, Neuro Oncol. 17 (2015) 639–651.

[76] L. Juillerat-Jeanneret, The targeted delivery of cancer drugs across the blood-brain barrier: chemical modifications of drugs or drug-nanoparticles? Drug Discov. Today 13 (2008) 1099–1106.

[77] F. Mo, A. Pellerino, R. Soffietti, R. Ruda, Blood-brain barrier in brain tumors: biology and clinical relevance, Int. J. Mol. Sci. 22 (2021) 12654.

[78] A. Estella-Hermoso de Mendoza, M. Rayo, F. Mollinedo, M.J. Blanco-Prieto, Lipid nanoparticles for alkyl lysophospholipid edelfosine encapsulation: development and in vitro characterization, Eur. J. Pharm. Biopharm. 68 (2008) 207–213.

[79] A. Estella-Hermoso de Mendoza, V. Preat, F. Mollinedo, M.J. Blanco-Prieto, *In vitro* and *in vivo* efficacy of edelfosine-loaded lipid nanoparticles against glioma, J. Control Release 156 (2011) 421–426.

[80] T. Nieto-Miguel, C. Gajate, F. Gonzalez-Camacho, F. Mollinedo, Proapoptotic role of Hsp90 by its interaction with c-Jun N-terminal kinase in lipid rafts in edelfosine-mediated antileukemic therapy, Oncogene 27 (2008) 1779–1787.

[81] J.A. Villa-Pulgarin, C. Gajate, J. Botet, A. Jimenez, N. Justies, R.E. Varela-M, A. Cuesta-Marban, I. Muller, M. Modolell, J.L. Revuelta, F. Mollinedo, Mitochondria and lipid raft-located F_OF_1-ATP synthase as major therapeutic targets in the antileishmanial and anticancer activities of ether lipid edelfosine, PLOS Negl. Trop. Dis. 11 (2017) e0005805.

[82] A. Ausili, A. Torrecillas, F.J. Aranda, F. Mollinedo, C. Gajate, S. Corbalan-Garcia, A. de Godos, J.C. Gomez-Fernandez, Edelfosine is incorporated into rafts and alters their organization, J. Phys. Chem. B 112 (2008) 11643–11654.

[83] V. Zaremberg, C. Gajate, L.M. Cacharro, F. Mollinedo, C.R. McMaster, Cytotoxicity of an anti-cancer lysophospholipid through selective modification of lipid raft composition, J. Biol. Chem. 280 (2005) 38047–38058.

[84] O. Czyz, T. Bitew, A. Cuesta-Marban, C.R. McMaster, F. Mollinedo, V. Zaremberg, Alteration of plasma membrane organization by an anticancer lysophosphatidylcholine analogue induces intracellular acidification and internalization of plasma membrane transporters in yeast, J. Biol. Chem. 288 (2013) 8419–8432.

[85] C. Abbal, M. Lambelet, D. Bertaggia, C. Gerbex, M. Martinez, A. Arcaro, M. Schapira, O. Spertini, Lipid raft adhesion receptors and Syk regulate selectin-dependent rolling under flow conditions, Blood 108 (2006) 3352–3359.

[86] T. Murai, Y. Maruyama, K. Mio, H. Nishiyama, M. Suga, C. Sato, Low cholesterol triggers membrane microdomain-dependent CD44 shedding and suppresses tumor cell migration, J. Biol. Chem. 286 (2011) 1999–2007.

[87] A. Girault, J.P. Haelters, M. Potier-Cartereau, A. Chantome, M. Pinault, S. Marionneau-Lambot, T. Oullier, G. Simon, H. Couthon-Gourves, P.A. Jaffres, B. Corbel, P. Bougnoux, V. Joulin, C. Vandier, New alkyl-lipid blockers of SK3 channels reduce cancer cell migration and occurrence of metastasis, Curr. Cancer Drug Targets 11 (2011) 1111–1125.

[88] M. Potier, V. Joulin, S. Roger, P. Besson, M.L. Jourdan, J.Y. Leguennec, P. Bougnoux, C. Vandier, Identification of SK3 channel as a new mediator of breast cancer cell migration, Mol. Cancer Ther. 5 (2006) 2946–2953.

[89] A. Chantome, A. Girault, M. Potier, C. Collin, P. Vaudin, J.C. Pages, C. Vandier, V. Joulin, KCa2.3 channel-dependent hyperpolarization increases melanoma cell motility, Exp. Cell Res. 315 (2009) 3620–3630.

[90] A. Chantome, M. Potier-Cartereau, L. Clarysse, G. Fromont, S. Marionneau-Lambot, M. Gueguinou, J.C. Pages, C. Collin, T. Oullier, A. Girault, F. Arbion, J. P. Haelters, P.A. Jaffres, M. Pinault, P. Besson, V. Joulin, P. Bougnoux, C. Vandier, Pivotal role of the lipid raft SK3-Orai1 complex in human cancer cell migration and bone metastases, Cancer Res. 73 (2013) 4852–4861.

[91] P.A. Jaffres, C. Gajate, A.M. Bouchet, H. Couthon-Gourves, A. Chantome, M. Potier-Cartereau, P. Besson, P. Bougnoux, F. Mollinedo, C. Vandier, Alkyl ether lipids, ion channels and lipid raft reorganization in cancer therapy, Pharmacol. Ther. 165 (2016) 114–131.

[92] F.J. Candal, D.C. Bosse, W.R. Vogler, E.W. Ades, Inhibition of induced angiogenesis in a human microvascular endothelial cell line by ET-18-OCH_3, Cancer Chemother. Pharmacol. 34 (1994) 175–178.

[93] W.R. Vogler, J. Liu, O. Volpert, E.W. Ades, N. Bouck, The anticancer drug edelfosine is a potent inhibitor of neovascularization *in vivo*, Cancer Investig. 16 (1998) 549–553.

[94] C. Gajate, F. Mollinedo, Biological activities, mechanisms of action and biomedical prospect of the antitumor ether phospholipid ET-18-OCH_3

(edelfosine), a proapoptotic agent in tumor cells, Curr. Drug Metab. 3 (2002) 491–525.
[95] F. Mollinedo, C. Gajate, S. Martin-Santamaria, F. Gago, ET-18-OCH_3 (edelfosine): a selective antitumour lipid targeting apoptosis through intracellular activation of Fas/CD95 death receptor, Curr. Med. Chem. 11 (2004) 3163–3184.
[96] J.P. Weichert, P.A. Clark, I.K. Kandela, A.M. Vaccaro, W. Clarke, M.A. Longino, A. N. Pinchuk, M. Farhoud, K.I. Swanson, J.M. Floberg, J. Grudzinski, B. Titz, A. M. Traynor, H.E. Chen, L.T. Hall, C.J. Pazoles, P.J. Pickhardt, J.S. Kuo, Alkylphosphocholine analogs for broad-spectrum cancer imaging and therapy, Sci. Transl. Med. 6 (2014) 240ra275.
[97] A.N. Pinchuk, M.A. Rampy, M.A. Longino, B.Y. Durkee, R.E. Counsell, J. P. Weichert, Effect of polar head group modifications on the tumor retention of phospholipid ether analogs: role of the quaternary nitrogen, Pharmaceutics 15 (2023) 171.
[98] R. Chen, E. Brady, T.M. McIntyre, Human TMEM30a promotes uptake of antitumor and bioactive choline phospholipids into mammalian cells, J. Immunol. 186 (2011) 3215–3225.
[99] F. Snyder, R. Wood, Alkyl and alk-1-enyl ethers of glycerol in lipids from normal and neoplastic human tissues, Cancer Res. 29 (1969) 251–257.
[100] Y. Gonzalez-Fernandez, E. Imbuluzqueta, M. Zalacain, F. Mollinedo, A. Patino-Garcia, M.J. Blanco-Prieto, Doxorubicin and edelfosine lipid nanoparticles are effective acting synergistically against drug-resistant osteosarcoma cancer cells, Cancer Lett. 388 (2017) 262–268.
[101] S.R. Vink, W.J. van Blitterswijk, J.H. Schellens, M. Verheij, Rationale and clinical application of alkylphospholipid analogues in combination with radiotherapy, Cancer Treat. Rev. 33 (2007) 191–202.
[102] M. Verheij, W.H. Moolenaar, W.J. Blitterswijk, Combining anti-tumor alkyl-phospholipid analogs and radiotherapy: rationale and clinical outlook, Anticancer Agents Med. Chem. 14 (2014) 618–628.
[103] A. Estella-Hermoso de Mendoza, M.A. Campanero, H. Lana, J.A. Villa-Pulgarin, J. de la Iglesia-Vicente, F. Mollinedo, M.J. Blanco-Prieto, Complete inhibition of extranodal dissemination of lymphoma by edelfosine-loaded lipid nanoparticles, Nanomedicine 7 (2012) 679–690.